ESAIM: M2AN 52 (2018) 965–993
https://doi.org/10.1051/m2an/2017040

ESAIM: Mathematical Modelling and Numerical Analysis
www.esaim-m2an.org

VIRTUAL ELEMENT METHOD FOR THE LAPLACE-BELTRAMI EQUATION ON SURFACES

Massimo Frittelli*,[1] and Ivonne Sgura[1]

Abstract. We present and analyze a Virtual Element Method (VEM) for the Laplace-Beltrami equation on a surface in $\mathbb{R}^3$, that we call Surface Virtual Element Method (SVEM). The method combines the Surface Finite Element Method (SFEM) (*Dziuk, Eliott, G. Dziuk and C.M. Elliott., Acta Numer. 22 (2013) 289–396.*) and the recent VEM (Beirão da Veiga *et al.*, *Math. Mod. Methods Appl. Sci. 23 (2013) 199–214.*) in order to allow for a general polygonal approximation of the surface. We account for the error arising from the geometry approximation and in the case of polynomial order $k = 1$ we extend to surfaces the error estimates for the interpolation in the virtual element space. We prove existence, uniqueness and first order H^1 convergence of the numerical solution.We highlight the differences between SVEM and VEM from the implementation point of view. Moreover, we show that the capability of SVEM of handling nonconforming and discontinuous meshes can be exploited in the case of surface pasting. We provide some numerical experiments to confirm the convergence result and to show an application of mesh pasting.

Mathematics Subject Classification. 65N15, 65N30.

Received December 2, 2016. Accepted August 21, 2017.

1. Introduction

The Virtual Element Method (VEM) is a recent extension of the well-known Finite Element Method (FEM) for the numerical approximation of several classes of partial differential equations on planar domains [1–7]. The main features of the method have been introduced in [1, 8]. The key feature of VEM is that of being a *polygonal* finite element method, *i.e.* the method handles elements of quite general polygonal shape, rather than just triangular [1], and nonconforming meshes [1, 9]. The increased mesh generality provides several advantages, we mention some of them. About nonconforming meshes: (i) they naturally arise when pasting several meshes to obtain a polygonal approximation of the whole domain [10, 11] and, in contrast to conforming pasting techniques [12, 13], there is no need to match the nodal points; (ii) they allow simple adaptive refinement strategies [14]. Elements of more general shape and arbitrary number of edges allow for: (i) flexible approximation of the domain and in particular of its boundary [15]; (ii) the possibility of enforcing higher regularity to the numerical solution [6, 16, 17].

Keywords and phrases. Surface PDEs, Laplace-Beltrami equation, surface finite element method, Virtual Element Method.

[1] Dipartimento di Matematica e Fisica E. De Giorgi, Università del Salento, via per Arnesano, 73100 Lecce, Italy.
* Corresponding author massimo.frittelli@unisalento.it

The core idea of the VEM is that, given a polynomial order $k \in \mathbb{N}$ and a polygonal element K, the local basis function space on K includes the polynomials of degree k (thus ensuring the optimal degree of accuracy) plus other basis functions that are not known in closed form [1]. The presence of these *virtual* functions motivates the name of the method. However, the knowledge of certain degrees of freedom attached to the basis functions is sufficient to compute the discrete bilinear forms with a degree of accuracy k.

The VEM introduced for the Laplace equation in two dimensions in the recent publication [1] has been extended to more complicated PDEs, for example a non exhaustive list of applications is: linear elasticity [2], plate bending [17], fracture problems [7], eigenvalue problems [3], Cahn-Hilliard equation [6], heat [4] and wave equations [5].

The aim of the present work is to consider the VEM in the case $k = 1$ and extend it to solve *surface PDEs*, *i.e.* PDEs having a two-dimensional smooth surface in $\mathbb{R}^3$ as spatial domain. Surface PDEs arise in the modelling of several problems such as advection [18], water waves [19], phase separation [20], reaction-diffusion systems and pattern formation [21–25], tumor growth [26], biomembrane modelling [27], cell motility [28], superconductivity [29], metal dealloying [30], image processing [21] and surface modelling [31].

Here we will focus on the *Laplace-Beltrami* equation, that is the prototypal second order elliptic PDE on smooth surfaces and corresponds to the extension of the Laplace equation to surfaces, see *e.g.* [32], (Chap. 14). Among the various discretisation techniques for surface PDEs existing in literature (see for example [24,26,33–38]) we consider the Surface Finite Element Method (SFEM) introduced in the seminal paper [39]. The core idea is to approximate the surface with a polygonal surface made, as in the planar case, of triangular non-overlapping elements whose vertices belong to the surface and to consider a space of piecewise linear functions. The resulting method is exactly similar to the well-known planar FEM, but the convergence estimates must account for the additional error arising from the approximation of the surface, see [37] for a thorough analysis of the method. In this paper, we define a Virtual Element Method on polygonal surfaces by combining the approaches of VEM and SFEM, we will refer to the resulting method as Surface Virtual Element Method (SVEM). Then we prove, under minimal regularity assumptions on the polygonal mesh, some error estimates for the approximation of surfaces and for the projection operators and bilinear forms involved in the method. Furthermore, we prove existence and uniqueness of the discrete solution and a first order (and thus optimal) H^1 error estimate. As an application, we show that SVEM can easily handle composite meshes arising from pasting two (or more) meshes along a curve in the space.

The structure of the paper is as follows. In Section 2, we recall some preliminaries on differential operators and function spaces on surfaces. In Section 3, we recall the Laplace-Beltrami equation on arbitrary smooth surfaces without boundary in strong and weak forms. In Section 4, we introduce a Virtual Element Method for the Laplace-Beltrami equation, defined on general polygonal approximation of surfaces. In Section 5, we prove error estimates for the discrete bilinear forms and the approximation of geometry. In Section 6, we prove existence, uniqueness and first order H^1 convergence of the numerical solution. In Section 7 we face with the issues related to the implementation of the method. In Section 8 we (i) discuss some advantages of the SVEM when applied to mesh pasting and (ii) present three numerical experiments on a sphere, a torus and a cylinder, respectively.

2. Differential operators on surfaces

In this section we recall some fundamental notions concerning surface PDEs. If not explicitly stated, definitions and results are taken from [37].

Definition 2.1 (C^k surface, normal and conormal vectors)**.** Given $k \in \mathbb{N}$, a set $\Gamma \subset \mathbb{R}^3$ is said to be a C^k *surface* if, for every $\mathbf{x}_0 \in \Gamma$, there exist an open set $U_{\mathbf{x}_0} \subset \mathbb{R}^3$ containing $\mathbf{x}_0$ and a function $\phi \in \mathrm{C}^k(U)$ such that

$$U_{\mathbf{x}_0} \cap \Gamma = \{\mathbf{x} \in U_{\mathbf{x}_0} | \phi(\mathbf{x}) = 0\}.$$

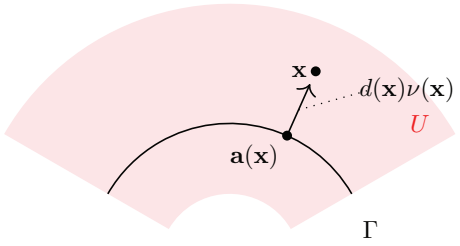

FIGURE 1. Surface Γ and respective Fermi stripe U. Each point $\mathbf{x} \in U$ is obtained by moving its normal projection $\mathbf{a}(\mathbf{x}) \in \Gamma$ by a distance $d(\mathbf{x})$ in the normal direction $\nu(\mathbf{x})$.

The vector field

$$\nu : \Gamma \to \mathbb{R}^3, \ \mathbf{x} \mapsto \frac{\nabla \phi(\mathbf{x})}{\|\nabla \phi(\mathbf{x})\|} \tag{2.1}$$

is said to be the *unit normal vector*. We denote by $\partial\Gamma$ the one-dimensional *boundary* of Γ. If $\partial\Gamma$ has a well-defined tangent direction at each point, the vector field $\mu : \partial\Gamma \to \mathbb{R}^3$ such that

- $\mu(\mathbf{x}) \perp \nu(\mathbf{x}) \quad \forall \mathbf{x} \in \partial\Gamma$;
- $\mu(\mathbf{x}) \perp \partial\Gamma \quad \forall \mathbf{x} \in \partial\Gamma$;
- $\mu(\mathbf{x})$ points outward of Γ,

is called the *conormal unit vector*.

Lemma 2.2 (Fermi coordinates, see [37])**.** *If Γ is a C^2 surface, there exists an open neighbourhood $U \subset \mathbb{R}^3$ of Γ such that every $\mathbf{x} \in U$ admits a unique decomposition of the form*

$$\mathbf{x} = \mathbf{a}(\mathbf{x}) + d(\mathbf{x})\nu(\mathbf{a}(\mathbf{x})), \qquad \mathbf{a}(\mathbf{x}) \in \Gamma, \ d(\mathbf{x}) \in \mathbb{R}. \tag{2.2}$$

The maximal open set U with this property is called the Fermi stripe *of Γ, $\mathbf{a}(\mathbf{x})$ is called* normal projection *onto Γ, $d(\mathbf{x})$ is called* oriented distance function *and $(\mathbf{a}(\mathbf{x}), d(\mathbf{x}))$ are called the* Fermi coordinates *of $\mathbf{x}$. An example of Fermi stripe is depicted in Figure 1.*

Definition 2.3 (Tangential gradient, tangential divergence)**.** If Γ is a C^1 surface, A is an open neighborhood of Γ and $f \in \mathrm{C}^1(A, \mathbb{R})$, the operator

$$\nabla_\Gamma f : \Gamma \to \mathbb{R}^3, \ \mathbf{x} \mapsto \nabla f(\mathbf{x}) - (\nabla f(\mathbf{x}) \cdot \nu(\mathbf{x}))\nu(\mathbf{x}) = P(\mathbf{x})\nabla f(\mathbf{x}), \tag{2.3}$$

where ∇ denotes the usual gradient in $\mathbb{R}^3$ and $P(\mathbf{x})_{ij} = \delta_{ij} - \nu_i(\mathbf{x})\nu_j(\mathbf{x})$, is called the *tangential gradient* of f. The components of the tangential gradient, *i.e.*

$$\underline{D}_i f : S \to \mathbb{R}, \ \mathbf{x} \mapsto P_i(\mathbf{x})\nabla f(\mathbf{x}), \qquad i \in \{1, 2, 3\}, \tag{2.4}$$

where $P_i(\mathbf{x})$ is the ith row of $P(\mathbf{x})$, are called the *tangential derivatives* of f. Given a vector field $F \in \mathrm{C}^1(A, \mathbb{R}^3)$, the operator

$$\nabla_\Gamma \cdot F : S \to \mathbb{R}, \ \mathbf{x} \mapsto \sum_{i=1}^{3} \underline{D}_i F_i(\mathbf{x}) \tag{2.5}$$

is called the *tangential divergence* of F.

Theorem 2.4. *Given $\Gamma \subset A$ a C^1 surface, if f and g are $\mathrm{C}^1(A,\mathbb{R})$ functions such that $f_{|\Gamma} = g_{|\Gamma}$, then*

$$\nabla_\Gamma f(\mathbf{x}) = \nabla_\Gamma g(\mathbf{x}) \quad \forall \mathbf{x} \in \Gamma.$$

This means that the tangential gradient of a function only depends on its restriction over Γ.

Theorem 2.4 makes the following definition well-posed.

Definition 2.5 ($\mathrm{C}^k(\Gamma)$ functions)**.** If Γ is a C^1 surface, a function $f : \Gamma \to \mathbb{R}$ is said to be $\mathrm{C}^1(\Gamma)$ if it is differentiable at any point of Γ and its tangential derivatives are continuous over Γ.

If $k \geq 2$ and Γ is a C^k surface, a function $f : \Gamma \to \mathbb{R}$ is said to be $\mathrm{C}^k(\Gamma)$ if it is $\mathrm{C}^1(\Gamma)$ and its tangential derivatives are $\mathrm{C}^{k-1}(\Gamma)$ functions.

Definition 2.6 (Laplace-Beltrami operator)**.** Given a C^2 surface Γ and $f \in \mathrm{C}^2(\Gamma)$, the operator

$$\Delta_\Gamma f : \Gamma \to \mathbb{R}, \ \mathbf{x} \mapsto \nabla_\Gamma \cdot \nabla_\Gamma f(\mathbf{x}) = \sum_{i=1}^{3} \underline{D}_i \underline{D}_i f(\mathbf{x})$$

is called the *Laplace-Beltrami* operator of f.

We now recall the definitions of some remarkable Sobolev spaces on surfaces.

Definition 2.7 (Sobolev spaces on surfaces)**.** Given $s \in \mathbb{N}$, let Γ be a C^s surface and let $\mathrm{L}^0(\Gamma)$ be the set of measurable functions with respect to the bidimensional Hausdorff measure on Γ. Consider the *Sobolev spaces*

$$\mathrm{H}^0(\Gamma) = \mathrm{L}^2(\Gamma) = \left\{ f \in \mathrm{L}^0(\Gamma) \;\middle|\; \int_\Gamma f^2 \, \mathrm{d}\sigma < +\infty \right\}; \tag{2.6}$$

$$\mathrm{H}^r(\Gamma) = \left\{ f \in \mathrm{L}^2(\Gamma) \mid \underline{D}_i f \in \mathrm{H}^{r-1}(\Gamma) \ \forall i \in \{1,2,3\} \right\}, \quad \forall \ 1 \leq r \leq s; \tag{2.7}$$

$$\mathrm{H}^r_0(\Gamma) = \left\{ f \in \mathrm{H}^r(\Gamma) \middle| \int_\Gamma f = 0 \right\}, \quad \forall \ 1 \leq r \leq s, \tag{2.8}$$

where derivatives are meant in distributional sense[2]. These are Hilbert spaces if endowed with the scalar products

$$\langle f, g \rangle_{\mathrm{H}^r(\Gamma)} = \int_\Gamma \left(\sum_{|\boldsymbol{\alpha}| \leq r} \underline{D}_{\boldsymbol{\alpha}} f \underline{D}_{\boldsymbol{\alpha}} g \right) \mathrm{d}\sigma \quad \forall f, g \in \mathrm{H}^r(\Gamma) \quad \forall \ 0 \leq r \leq s.$$

where $\underline{D}_{\boldsymbol{\alpha}}$ is the multi-index notation for partial tangential derivatives, see [41].

Norms will be denoted by $\| \cdot \|_{\mathrm{L}^2(\Gamma)}$, $\| \cdot \|_{\mathrm{H}^r(\Gamma)}$ and seminorms by $| \cdot |_{\mathrm{H}^r(\Gamma)}$.

As well as in the planar case, a Poincaré inequality holds on $\mathrm{H}^1_0(\Gamma)$, see [37].

Theorem 2.8 (Poincaré's inequality on surfaces)**.** *Given a C^2 surface Γ with a well-defined tangent vector field on the boundary $\partial\Gamma$, there exists $C > 0$ such that*

$$\|f\|_{\mathrm{L}^2(\Gamma)} \leq C |f|_{\mathrm{H}^1(\Gamma)} \qquad \forall \ f \in \mathrm{H}^1_0(\Gamma). \tag{2.9}$$

A basic result in surface calculus, taken from [37], is the following

Theorem 2.9 (Green's formula on surfaces)**.** *Given a C^2 surface Γ with a well-defined tangent vector field on the boundary $\partial\Gamma$ and $f, g \in \mathrm{C}^2(\Gamma)$, it holds that*

$$\int_\Gamma f \Delta_\Gamma g \, \mathrm{d}\sigma = -\int_\Gamma \nabla_\Gamma f \cdot \nabla_\Gamma g \, \mathrm{d}\sigma + \int_{\partial\Gamma} f \frac{\partial g}{\partial \mu} \, \mathrm{d}l, \tag{2.10}$$

where μ is the conormal vector (see Def. 2.1) and $\frac{\partial g}{\partial \mu}(\mathbf{x}) := \nabla_\Gamma g(\mathbf{x}) \cdot \mu(\mathbf{x})$ is the conormal derivative *of g on $\partial\Gamma$.*

[2] See [40], (Chap. 4) or [37], (Def. 2.11) for a precise definition of distributional tangential derivatives.

3. The Laplace-Beltrami equation

In this section we introduce the Laplace-Beltrami equation on a surface without boundary, that will be the model problem throughout the paper.

Let Γ be a C^3 surface without boundary and let $f \in L^2(\Gamma)$ such that $\int_\Gamma f = 0$. Consider the Laplace-Beltrami equation on Γ, given by

$$\begin{cases} -\Delta_\Gamma u(\mathbf{x}) = f(\mathbf{x}), & \mathbf{x} \in \Gamma, \\ \int_\Gamma u(\mathbf{x})\, d\mathbf{x} = 0, \end{cases} \tag{3.1}$$

and its weak formulation

$$\begin{cases} u \in H_0^1(\Gamma) \\ a(u,\phi) = \langle f, \phi \rangle_{L^2(\Gamma)} \qquad \forall\, \phi \in H^1(\Gamma), \end{cases} \tag{3.2}$$

where $a(u,v) := \int_\Gamma \nabla_\Gamma u \cdot \nabla_\Gamma v$ for all $u, v \in H^1(\Gamma)$ and $\langle u, v \rangle_{L^2(\Gamma)} := \int_\Gamma uv$ for all $u, v \in L^2(\Gamma)$. Notice that, from condition $\int_\Gamma f = 0$, the formulation (3.2) is equivalent to

$$\begin{cases} u \in H_0^1(\Gamma) \\ a(u,\phi) = \langle f, \phi \rangle_{L^2(\Gamma)} \qquad \boxed{\forall\, \phi \in H_0^1(\Gamma).} \end{cases} \tag{3.3}$$

Let us justify the above requirements $\int_\Gamma u = 0$ and $\int_\Gamma f = 0$. Since $\phi \equiv 1$ is allowed as a test function for the weak Laplace-Beltrami equation (3.2), it follows $\int_\Gamma f = 0$ as a compatibility condition. Moreover, if u fulfills $a(u,\phi) = \langle f, \phi \rangle_{L^2(\Gamma)}$ $\forall \phi \in H^1(\Gamma)$ and $c \in \mathbb{R}$, then $u + c$ fulfills the same equation; condition $\int_\Gamma u = 0$ is thus enforced to provide uniqueness of the solution. Existence and uniqueness for problem (3.3) will be proven rigorously in Theorem 6.1 in Section 6.

Remark 3.1 (Surfaces with boundary)**.** The whole analysis carried out in this paper holds unchanged in the presence of a non-empty boundary, $\partial\Gamma \neq \emptyset$, and homogeneous Neumann boundary conditions. In the case of homogeneous Dirichlet boundary conditions, the analysis still holds if $H_0^1(\Gamma)$ is the space of $H^1(\Gamma)$ functions that vanish on $\partial\Gamma$ in a weak sense, see [40], (Chap. 4.5).

4. Space discretisation by SVEM

In this section, we will address space discretisation of (3.3). After defining the approximation of the geometry and the corresponding discrete function spaces, the Surface Virtual Element Method (SVEM) will be introduced.

4.1. Approximation of the surface

In this section, we define a polygonal approximation of the surface Γ in Definition 2.1 and a *virtual element* space on this polygonal approximation. The method will thus generalise, in the piecewise linear case, the Surface Finite Element Method (SFEM) [37] and the Virtual Element Method (VEM) [1] at once.

Given a C^2 surface Γ in $\mathbb{R}^3$, we constuct a piecewise flat approximate surface Γ_h, defined as

$$\Gamma_h = \bigcup_{E \in \mathcal{T}_h} E, \tag{4.1}$$

where:

(1) $\mathcal{T}_h$ is a finite set of non-overlapping simple polygons, *i.e.* without holes and with non self-intersecting boundary, having diameters less than or equal to $h > 0$;
(2) Γ_h is contained in the Fermi stripe U associated to Γ, see Lemma 2.2;
(3) The normal projection $\mathbf{a} : \Gamma_h \to \Gamma$ defined in Lemma 2.2 is one-to-one;

(4) the vertices of Γ_h lie on Γ.

Following [37], we define how to lift functions from the approximate surface Γ_h to the continuous one Γ.

Definition 4.1 (Lifted functions)**.** Let Γ be a C^2 surface and Γ_h be as in (4.1). Given a function $\phi : \Gamma_h \to \mathbb{R}$, its *lift* $\phi^\ell : \Gamma \to \mathbb{R}$ is defined by $\phi \circ (\mathbf{a}_{|\Gamma_h})^{-1}$, where $\mathbf{a} : \Gamma_h \to \Gamma$ is the normal projection defined in Lemma 2.2. Given a function $\psi : \Gamma \to \mathbb{R}$, its *unlift* $\psi^{-\ell} : \Gamma_h \to \mathbb{R}$ is defined by $\psi \circ \mathbf{a}$.

This definition is well-posed thanks to assumption (3).

Furthermore, the following mesh regularity requirements will be assumed throughout the paper. There exist $\gamma_1, \gamma_2 > 0$ such that, for all $h > 0$ and $E \in \mathcal{T}_h$,

(A1) E is star-shaped with respect to a ball of radius ρ_E such that

$$\rho_E \geq \gamma_1 h_E;$$

(A2) for every pair of nodes $P, Q \in E$, the distance $\|P - Q\|$ fulfills

$$\|P - Q\| \geq \gamma_2 h_E,$$

where h_E is the diameter of E.

Remark 4.2. This kind of polygonal approximation has two remarkable subcases:

(1) If each $E \in \mathcal{T}_h$ has three vertices, we obtain the classical triangulations adopted, for instance, in [37,39].
(2) If Γ is a flat surface, we obtain the polygonal meshes considered in [1].

We remark that the considered class of polygonations includes nonconforming meshes. We will show in Section 8.1 that this feature can be exploited in mesh pasting.

4.2. Discrete function spaces

In this subsection we define local function spaces based on the paper [42], which treats the VEM in the planar case. For our purpose, the standard gradient operator used for defining the function spaces is replaced by the tangential gradient on the polygonal surface. Consider $E \in \mathcal{T}_h$. Without loss of generality, E may be assumed to lie in the (x, y) plane. We consider the space

$$\tilde{V}_h(E) = \{v_h \in \mathrm{H}^1(E) \mid v_{h|e} \in \mathbb{P}_1(e)\ \forall e\ \in \mathrm{edges}(E),\ \Delta v_h \in \mathbb{P}_1(E)\}. \tag{4.2}$$

We recall that functions in $\tilde{V}_h(E)$ are *virtual*, *i.e.* they are not known explicitly. For this reason we consider the projection $\Pi_E^\nabla : V_h(E) \to \mathbb{P}_1(E)$ defined by

$$\int_E \nabla_E \Pi_E^\nabla(v_h) \cdot \nabla_E q_1 = \int_E \nabla_E v_h \cdot \nabla_E q_1 \qquad \forall\ q_1 \in \mathbb{P}_1(E); \tag{4.3}$$

$$\sum_{P \in\ \mathrm{nodes}(E)} \Pi_E^\nabla v_h(P) = \sum_{P \in\ \mathrm{nodes}(E)} v_h(P), \tag{4.4}$$

where (4.4) is needed to fix the free constant in (4.3). Exactly as in the case of planar domains considered in [1], this projection is computable. The *local virtual space* is defined by

$$V_h(E) := \left\{ v_h \in \tilde{V}_h(E) \middle| \int_E (v_h - \Pi_E^\nabla v_h) q_1 = 0\ \forall q_1 \in \mathbb{P}_1(E) \right\}. \tag{4.5}$$

In [42] it has been proven that the nodal values

$$\{v_h(P) | P \in \mathrm{vertices}(E)\} \tag{4.6}$$

are unisolvent for the space $V_h(E)$ in (4.5). Given $w \in \mathrm{H}^s(E)$, $s > 1$, by Sobolev's embedding theorem we have $w \in \mathrm{C}^0(E)$. Hence, the nodal values of w are well-defined. The unique function $w_I \in V_h(E)$ such that

$$w_I(P) = w(P), \qquad P \in \text{vertices}(E), \tag{4.7}$$

is said to be the *interpolant* of w. If $\tilde{E} = \mathbf{a}(E)$ is the curved element corresponding to E and $v \in \mathrm{H}^2(\tilde{E})$, we have $v^{-\ell} \in \mathrm{H}^2(E)$, for this result see Theorem 5.4 in Section 5. The unique function $v_I \in V_h(E)$ such that

$$v_I(P) = v^{-\ell}(P), \qquad P \in \text{vertices}(E), \tag{4.8}$$

is said to be the interpolant of v.

Remark 4.3. From the definition of $V_h(E)$ in (4.5) it follows that:

(1) $\mathbb{P}_1(E) \subseteq V_h(E)$;
(2) every $v_h \in V_h(E)$ is explicitly known on the boundary ∂E, but not on the interior $\mathring{E}$;
(3) if E is a triangle, $V_h(E) = \mathbb{P}_1(E)$, *i.e.* the VEM method reduces to FEM.

The global discrete space will be defined by

$$V_h = \{v_h \in \mathrm{C}^0(\Gamma_h) \mid v_{h|E} \in V_h(E) \ \forall\ E \in \mathcal{T}_h\}.$$

Furthermore, we define the zero-averaged virtual space W_h by

$$W_h = \left\{ v_h \in V_h \;\middle|\; \int_{\Gamma_h} v_h = 0 \right\}. \tag{4.9}$$

We observe that, from definition (4.5), the integral in (4.9) is computable. Finally, we define the following broken H^s seminorms, $s \in \{1, 2\}$, on the polygonal surface Γ_h:

$$|v_h|_{h,s} = \sqrt{\sum_{E \in \mathcal{T}_h} |v_{h|E}|^2_{\mathrm{H}^s(E)}} \qquad \forall v_h \in \prod_{E \in \mathcal{T}_h} \mathrm{H}^s(E)$$

4.3. The Surface Virtual Element Method

We may write a discrete formulation for (3.3):

$$\begin{cases} u_h \in W_h \\ \int_{\Gamma_h} \nabla_{\Gamma_h} u_h \cdot \nabla_{\Gamma_h} \phi_h = \int_{\Gamma_h} f_I \phi_h \qquad \forall\ \phi_h \in W_h. \end{cases} \tag{4.10}$$

where f_I is the interpolant of f defined piecewise in (4.8). For later purposes, we define $\bar{a}(u_h, v_h) := \int_{\Gamma_h} \nabla_{\Gamma_h} u_h \cdot \nabla_{\Gamma_h} v_h$ for all $u_h, v_h \in W_h$ and $\langle u_h, v_h \rangle_{\mathrm{L}^2(\Gamma_h)} := \int_{\Gamma_h} u_h v_h$ for all $u_h \in \mathrm{L}^2(\Gamma_h)$ and $v_h \in W_h$.

Remark 4.4 (Regularity of f)**.** In the following we assume $f \in \mathrm{H}^2(\Gamma)$, such that, from Sobolev's embedding theorem, its pointwise values (and thus its interpolant f_I) are well-defined. We remark that, in the framework of surface PDEs, the problem of numerically handling $\mathrm{H}^s(\Gamma)$, $0 \le s \le 1$, load terms is intrinsically challenging. In fact, if the pointwise values of f are not available, then any approximation $\bar{f}$ of f defined on Γ_h must account for the mapping $\mathbf{a} : \Gamma_h \to \Gamma$ in (2.2) that, in general, is not computable.

Notice that $\bar{a}(\cdot, \cdot)$ and $\langle f_I, \cdot \rangle_{\mathrm{L}^2(\Gamma_h)}$ are not computable. We thus need to write a computable approximation of problem (4.10). To this end, following [1], an approximate bilinear form $a_h(\cdot, \cdot)$ and an approximate linear form $\langle f_h, \cdot \rangle_h$ will be constructed instead of $\bar{a}(\cdot, \cdot)$ and $\langle f_I, \cdot \rangle_{\mathrm{L}^2(\Gamma_h)}$, respectively.

For each $E \in \mathcal{T}_h$, we consider the local form $\bar{a}_E(v_h, w_h) := \int_E \nabla_E v_h \cdot \nabla_E w_h$, for all $v_h, w_h \in V_h(E)$. Following [1], we consider a local approximate form defined by

$$a_{h,E}(v_h, w_h) = \bar{a}_E\left(\Pi_E^\nabla v_h, \Pi_E^\nabla w_h\right) + S_E\left(\left(I - \Pi_E^\nabla\right) v_h, \left(I - \Pi_E^\nabla\right) w_h\right) \qquad \forall\, v_h, w_h \in V_h(E), \tag{4.11}$$

where S_E is a stabilising form defined by

$$S_E(v_h, w_h) = \sum_{\mathbf{x}_i \in \text{nodes}(E)} v_h(\mathbf{x}_i) w_h(\mathbf{x}_i) \qquad \forall\, v_h, w_h \in V_h(E), \tag{4.12}$$

which scales as $\bar{a}_E$ on the kernel of Π_E^∇, (see [1]) *i.e.* there exist $c^* > c_* > 0$ such that

$$c_* \bar{a}_E(v_h, v_h) \le S_E(v_h, v_h) \le c^* \bar{a}_E(v_h, v_h) \qquad \forall\, v_h \in \ker\left(\Pi_E^\nabla\right). \tag{4.13}$$

Notice that, since $\Pi_E^\nabla q_1 = q_1$ for all $q_1 \in \mathbb{P}_1(E)$, the local form (4.11) fulfils the consistency property

$$a_{h,E}(v_h, q_1) = \bar{a}_E(v_h, q_1) \qquad \forall v_h \in V_h(E), \qquad \forall q_1 \in \mathbb{P}_1(E). \tag{4.14}$$

A global approximate gradient form is defined by pasting the local ones:

$$a_h(v_h, w_h) := \sum_{E \in \mathcal{T}_h} a_{h,E}(v_{h|E}, w_{h|E}) \qquad \forall\, v_h, w_h \in V_h. \tag{4.15}$$

We want to define an approximate L^2 form and the approximate right hand side. For each $E \in \mathcal{T}_h$, consider the local $\mathrm{L}^2(E)$ projection $\Pi_E^0 : V_h(E) \to \mathbb{P}_1(E)$ given by

$$\langle \Pi_E^0 v_h, q_1 \rangle_{\mathrm{L}^2(E)} = \langle v_h, q_1 \rangle_{\mathrm{L}^2(E)} \qquad \forall q_1 \in \mathbb{P}_1(E). \tag{4.16}$$

We remark that $\Pi_E^0 = \Pi_E^\nabla$ (see for instance [42] for the planar case), hence Π_E^0 is computable. Following [8], and in analogy with the approximate gradient form (4.11), we consider the following local approximate L^2 form:

$$\langle v_h, w_h \rangle_{\mathrm{L}^2_{h,E}} := \int_{\Gamma_h} \Pi_E^0 v_h \Pi_E^0 w_h + |E| S_E((I - \Pi_E^0) v_h, (I - \Pi_E^0) w_h) \qquad \forall v_h, w_h \in V_h(E), \tag{4.17}$$

where S_E and Π_E^0 are defined in (4.12) and (4.16), respectively. Notice that the local approximate L^2 form (4.17) fulfils the consistency property

$$\langle v_h, q_1 \rangle_{\mathrm{L}^2_h,E} = \langle v_h, q_1 \rangle_{\mathrm{L}^2(E)} \qquad \forall v_h \in V_h(E), \qquad \forall q_1 \in \mathbb{P}_1(E).$$

As a consequence, we have that

$$\langle v_h, 1 \rangle_{\mathrm{L}^2_h,E} = \int_E v_h \qquad \forall v_h \in V_h(E), \tag{4.18}$$

i.e. the integral of any $V_h(E)$ function can be computed exactly. A computable global approximate L^2 form is obtained by pasting the local ones:

$$\langle v_h, w_h \rangle_{\mathrm{L}^2_h} = \sum_{E \in \mathcal{T}_h} \langle v_{h|E}, w_{h|E} \rangle_{\mathrm{L}^2_h,E} \qquad \forall v_h, w_h \in V_h. \tag{4.19}$$

Property (4.18) implies that the space W_h defined in (4.9) can be represented as

$$W_h = \{v_h \in V_h | \langle v_h, 1 \rangle_{\mathrm{L}^2_h} = 0\}, \tag{4.20}$$

hence W_h is computable. To approximate the right hand side, following [1], for any function $g \in \mathrm{H}^1(\Gamma_h)$ we consider the functional $\langle g, \cdot \rangle_h$ defined by

$$\langle g, v_h \rangle_h = \sum_{E \in \mathcal{T}_h} \int_E g \sum_{V \in \text{vertices}(E)} \frac{v_h(V)}{n_E} \qquad \forall\, v_h \in V_h, \tag{4.21}$$

where n_E is the number of vertices of E. From (4.18) we have that $\langle g, v_h \rangle_h$ is computable, given the degrees of freedom of g and v_h. Furthermore, notice that

$$\langle g, 1 \rangle_h = \int_{\Gamma_h} g \qquad \forall g \in \mathrm{H}^1(\Gamma). \tag{4.22}$$

Another difference between the presented method and its planar counterpart introduced in [1] is the approximation of the load term. In fact, as well as in the continuous formulation (3.3), the numerical method needs a zero-averaged load term in order to be well-posed. To this end, we define the load term

$$f_h := f_I - \frac{\langle f_I, 1 \rangle_{\mathrm{L}^2_h}}{|\Gamma_h|}. \tag{4.23}$$

From (4.18), f_h is zero averaged and, from (4.22), f_h fulfils

$$\langle f_h, 1 \rangle_h = 0. \tag{4.24}$$

We may now write a computable discrete problem, as follows:

$$\begin{cases} u_h \in W_h \\ a_h(u_h, \phi_h) = \langle f_h, \phi_h \rangle_h \qquad \forall\, \phi_h \in W_h. \end{cases} \tag{4.25}$$

We will discuss the implementation of (4.25) in Section 7, while the error analysis will be carried out in next sections in the following steps, respectively:

(1) the geometric and interpolation error estimates in [37] will be extended to our polygonal/virtual setting;
(2) the error between the continuous weak formulation (3.3) and the computable discrete one (4.25) will be estimated by extending the analogous convergence theorem in [1] to surfaces.

In Section 5 we deal with step (1), in Section 6 we deal with step (2).

5. Interpolation, projection and geometric error estimates

We start this section by recalling some results. The following result taken from [43] addresses the projection error on $\mathbb{P}_1(E)$, $E \in \mathcal{T}_h$.

Theorem 5.1. *Under the regularity Assumption (A1), there exists $C > 0$, depending only on Γ, such that for $s \in \{1, 2\}$ and for all $w \in \mathrm{H}^s(E)$ there exists a $w_\pi \in \mathbb{P}_1(E)$ such that*

$$\|w - w_\pi\|_{\mathrm{L}^2(E)} + h_E |w - w_\pi|_{\mathrm{H}^1(E)} \leq C h_E^s |w|_{\mathrm{H}^s(E)}. \tag{5.1}$$

We now address interpolation in $V_h(E)$, $E \in \mathcal{T}_h$. The following theorem from [1] gives an interpolation error estimate in $V_h(E)$.

Theorem 5.2. *Under the regularity Assumption (A1), there exists $C > 0$, depending only on Γ, such that for all $w \in \mathrm{H}^2(E)$, the interpolant $w_I \in V_h(E)$ satisfies*

$$\|w - w_I\|_{\mathrm{L}^2(E)} + h |w - w_I|_{\mathrm{H}^1(E)} \leq C h_E^2 |w|_{\mathrm{H}^2(E)}. \tag{5.2}$$

To approximate integrals and bilinear forms under lifting, a geometric error must be taken into account. To this end, we recall some geometric quantities from [37]. For any $\mathbf{x} \in \Gamma_h$, let B_ε be an open ball (in the topology of Γ_h) centred in $\mathbf{x}$ with radius ε. Define

$$\delta_h(\mathbf{x}) := \lim_{\varepsilon \to 0} \frac{\mathrm{meas}(\mathbf{a}(B_\varepsilon))}{\mathrm{meas}(B_\varepsilon)}, \qquad \mathbf{x} \in \Gamma_h, \tag{5.3}$$

where meas denotes the two-dimensional Hausdorff measure. Let P and P_h be the projections onto the tangent planes of the smooth and the discrete surfaces, respectively, that is $P_{ij} = \delta_{ij} - \nu_i \nu_j$ and $P_{h,ij} = \delta_{ij} - \nu_{h,i}\nu_{h,j}$ for $i, j = 1, 2, 3$, and define

$$\mathcal{Q}_h = \frac{1}{\delta_h} P(I - d\mathcal{H})P_h(I - d\mathcal{H})P, \tag{5.4}$$

where d is the oriented distance function defined in (2.2) and $\mathcal{H}$ is the Weingarten map defined by $\mathcal{H}_{ij} = \underline{D}_i \nu_j$ for $i, j = 1, 2, 3$. The analysis of the geometric error will rely on the following fundamental equalities borrowed from [37]:

$$\int_\Gamma u^\ell v^\ell - \int_{\Gamma_h} uv = \int_\Gamma \left(1 - \frac{1}{\delta_h^\ell}\right) u^\ell v^\ell, \qquad \forall u, v \in \mathrm{L}^2(\Gamma_h) \text{ s.t. } u^\ell, v^\ell \in \mathrm{L}^2(\Gamma); \tag{5.5}$$

$$\int_\Gamma \nabla_\Gamma u^\ell \cdot \nabla_\Gamma v^\ell - \int_{\Gamma_h} \nabla_{\Gamma_h} u \cdot \nabla_{\Gamma_h} v = \int_\Gamma (P - \mathcal{Q}_h) \nabla_\Gamma u^\ell \cdot \nabla_\Gamma v^\ell, \qquad \forall u, v \in \mathrm{H}^1(\Gamma_h) \text{ s.t. } u^\ell, v^\ell \in \mathrm{H}^1(\Gamma). \tag{5.6}$$

Relations (5.5)–(5.6) motivate the following lemma, which generalises Lemma 4.1 in [37] to polygonal approximations of the surface.

Lemma 5.3. *Let Γ_h be a polygonal approximation of Γ as in (4.1). The oriented distance function introduced in (2.2) fulfils*

$$\|d\|_{\mathrm{L}^\infty(\Gamma_h)} \leq Ch^2. \tag{5.7}$$

The surface measure quotient δ_h defined in (5.3) fulfils

$$\|1 - \delta_h\|_{\mathrm{L}^\infty(\Gamma_h)} \leq Ch^2. \tag{5.8}$$

The following estimate holds

$$\|P - \mathcal{Q}_h\|_{\mathrm{L}^\infty(\Gamma_h)} \leq Ch^2. \tag{5.9}$$

In all of the claimed inequalities C depends only on the curvature of Γ.

Proof. We start by recalling the definition of the $|\cdot|_{\mathcal{C}^2}$ seminorm on polygons and segments. Let U be an open set in $\mathbb{R}^3$, let E be a polygon contained in U and let r be a segment contained in E. Without loss of generality, E and r may be assumed to lie in $\mathbb{R}^2$ and $\mathbb{R}$, respectively. Let $u \in \mathcal{C}^2(U)$. Then consider

$$|u|_{\mathcal{C}^2(r)} := \max_{x \in r} \left| \frac{\partial^2 u}{\partial x^2}(x) \right|, \quad |u|_{\mathcal{C}^2(E)} := \max_{\substack{\boldsymbol{\alpha} \in (\mathbb{N} \cup 0)^2 \\ |\boldsymbol{\alpha}| = 2}} \max_{\mathbf{x} \in E} \left| \frac{\partial^2 u}{\partial \mathbf{x}^{\boldsymbol{\alpha}}}(\mathbf{x}) \right|, \quad |u|_{\mathcal{C}^2(U)} := \max_{\substack{\boldsymbol{\alpha} \in (\mathbb{N} \cup 0)^3 \\ |\boldsymbol{\alpha}| = 2}} \max_{\mathbf{x} \in U} \left| \frac{\partial^2 u}{\partial \mathbf{x}^{\boldsymbol{\alpha}}}(\mathbf{x}) \right|,$$

with the multi-index notation for partial derivatives. It is easy to prove that

$$|u|_{\mathcal{C}^2(r)} \leq |u|_{\mathcal{C}^2(E)} \leq |u|_{\mathrm{C}^2(U)}. \tag{5.10}$$

Furthermore, if u_r is the linear interpolant of u on r, *i.e.* the linear function on r that agrees with u at the endpoints of r, the following classical interpolation error estimate holds

$$\|u - u_r\|_{\mathrm{L}^\infty(r)} \leq C|r|^2 |u|_{\mathrm{C}^2(r)}, \tag{5.11}$$

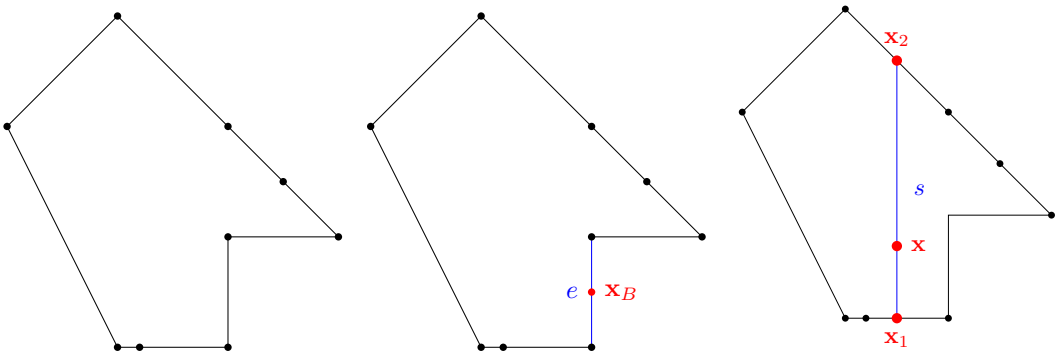

(a) The element E is given.

(b) The point x_B is on the edge e of the boundary ∂E.

(c) $\mathbf{x}_1$ and $\mathbf{x}_2$ are two distinct intersection points between s and ∂E such that $[\mathbf{x}_1, \mathbf{x}_2] \subset E$.

FIGURE 2. Some steps of the proof of Lemma 5.3.

where $|r|$ is the length of r, see [44]. Consider $E \in \mathcal{T}_h$, see Figure 5. First of all we prove that

$$\|d\|_{\mathrm{L}^\infty(\partial E)} \leq Ch^2 |d|_{\mathrm{C}^2(E)}. \tag{5.12}$$

To this end, let $\mathbf{x}_B \in \partial E$ and let e be an edge of E such that $\mathbf{x}_B \in e$, see Figure 5. Then, if d_e is the linear interpolant of d on e, then (i) $d_e \equiv 0$ since d vanishes at the endpoints of e and (ii) the interpolation error estimate (5.11) holds with $r = e$ and $u = d$. Using also (5.10), we have

$$|d(\mathbf{x}_B)| \leq \|d_e\|_{\mathrm{L}^\infty(e)} + \|d - d_e\|_{\mathrm{L}^\infty(e)} \leq C|e|^2 |d|_{\mathrm{C}^2(e)} \leq Ch^2 |d|_{\mathrm{C}^2(E)},$$

that proves (5.12). Now let $\mathbf{x} \in \mathring{E}$ and let s be any straight line contained in the plane of E and passing through $\mathbf{x}$, let $\mathbf{x}_1, \mathbf{x}_2 \in s \cap \partial E$ such that $[\mathbf{x}_1, \mathbf{x}_2] \subset E$, see Figure 5, and let d_s be the linear interpolant of d on s. By choosing $r = s$ and $u = d$ in (5.11), using (5.10) and (5.12) we have that

$$\begin{aligned} |d(\mathbf{x})| &\leq \|d_s\|_{\mathrm{L}^\infty(s)} + \|d - d_s\|_{\mathrm{L}^\infty(s)} = \max(|d(\mathbf{x}_1)|, |d(\mathbf{x}_2)|) + \|d - d_s\|_{\mathrm{L}^\infty(s)} \\ &\leq \|d\|_{\mathrm{L}^\infty(\partial E)} + C|s|^2 |d|_{\mathrm{C}^2(s)} \leq Ch^2 |d|_{\mathrm{C}^2(E)} \leq Ch^2 |d|_{\mathrm{C}^2(U)}, \end{aligned} \tag{5.13}$$

where U is the Fermi stripe of Γ. Now, $|d|_{\mathrm{C}^2(U)}$ depends only on the curvature of Γ, thus (5.13) proves (5.7). To prove (5.7), (5.8) and (5.9), we proceed as in Lemma 4.1 in [37] using estimate (5.7) for polygonal meshes. □

The following lemma generalizes Lemma 4.2 in [37] to our polygonal setting and provides lower and upper bounds for some norms of arbitrary functions when they are unlifted from Γ to Γ_h or lifted from Γ_h to Γ.

Lemma 5.4. *Let $w : \Gamma_h \to \mathbb{R}$ with lift $w^\ell : \Gamma \to \mathbb{R}$. Let $\mathbf{a} : \Gamma_h \to \Gamma$ be the projection onto Γ defined in (2.2) and, for every $E \in \mathcal{T}_h$, let $\tilde{E} = \mathbf{a}(E) \subset \Gamma$ be the curved element corresponding to $E \in \mathcal{T}_h$. Then*

$$\frac{1}{C}\|w\|_{\mathrm{L}^2(E)} \leq \|w^\ell\|_{\mathrm{L}^2(\tilde{E})} \leq C\|w\|_{\mathrm{L}^2(E)}; \tag{5.14}$$

$$\frac{1}{C}\|\nabla_E w\|_{\mathrm{L}^2(E)} \leq \|\nabla_{\tilde{E}} w^\ell\|_{\mathrm{L}^2(\tilde{E})} \leq C\|\nabla_E w\|_{\mathrm{L}^2(E)}; \tag{5.15}$$

$$\|\nabla_E^2 w\|_{\mathrm{L}^2(E)} \leq C\|\nabla_{\tilde{E}}^2 w^\ell\|_{\mathrm{L}^2(\tilde{E})} + Ch_E\|\nabla_{\tilde{E}} w^\ell\|_{\mathrm{L}^2(\tilde{E})}, \tag{5.16}$$

if the norms exist, where C depends only on the local metric and the curvature tensors of Γ.

Proof. We use the estimates of Lemma 5.3 for polygonal meshes into (5.5)–(5.6) and proceed exactly as in [37], (Lem. 4.2). □

Notice that Equations (5.14) and (5.15) express the following equivalences under lifting: (5.14) between $\mathrm{L}^2(\Gamma_h)$ and $\mathrm{L}^2(\Gamma)$ norms and (5.15) between $\mathrm{H}^1(\Gamma_h)$ and $\mathrm{H}^1(\Gamma)$ seminorms. Equation (5.16) can be interpreted as an h-perturbed dominance of the $\mathrm{H}^2(\Gamma)$ seminorm over the $\mathrm{H}^2(\Gamma_h)$ seminorm.

The following result provides error estimates for the interpolation in V_h^ℓ and the projection on $\left(\prod_E \mathbb{P}_1(E)\right)^\ell$. The interpolation result extends to SVEM Lemma 4.3 in [37] for the triangular SFEM.

Theorem 5.5. *Given a* C^2 *surface* Γ*, there exists* $C > 0$ *such that, for all* $v \in \mathrm{H}^2(\Gamma)$ *and* $w \in \mathrm{H}^s(\Gamma)$*,* $s \in \{1, 2\}$*, and for all* $h > 0$*, then*

- *the interpolant* $v_I \in V_h^1$ *fulfills*

$$\|v - v_I^\ell\|_{\mathrm{L}^2(\Gamma)} + h|v - v_I^\ell|_{\mathrm{H}^1(\Gamma)} \leq Ch^2 \left(|v|_{\mathrm{H}^2(\Gamma)} + h|v|_{\mathrm{H}^1(\Gamma)}\right); \tag{5.17}$$

- *there exists a projection* $w_\pi \in \prod_E \mathbb{P}_1(E)$ *such that*

$$\|w - w_\pi^\ell\|_{\mathrm{L}^2(\Gamma)} + h|w - w_\pi^\ell|_{h,1} \leq Ch^s \left(|w|_{\mathrm{H}^s(\Gamma)} + h|w|_{\mathrm{H}^1(\Gamma)}\right). \tag{5.18}$$

Proof. From Lemma 5.4, $w^{-\ell} \in \mathrm{H}^1(\Gamma_h) \cap \prod_E \mathrm{H}^s(E)$. Let w_π be the $\prod_E \mathbb{P}_1(E)$ projection of $w^{-\ell}$ as in (5.1) and let v_I be the V_h^1 interpolant of $v^{-\ell}$ defined piecewise by (4.7). From Theorems 5.1 and 5.2, by summing piecewise contributions, we have

$$\|w^{-\ell} - w_\pi\|_{\mathrm{L}^2(\Gamma_h)} + h|w^{-\ell} - w_\pi|_{h,1} \leq Ch^s |w^{-\ell}|_{2,h}, \tag{5.19}$$

$$\|v^{-\ell} - v_I\|_{\mathrm{L}^2(\Gamma_h)} + h|v^{-\ell} - v_I|_{\mathrm{H}^1(\Gamma_h)} \leq Ch^2 |v^{-\ell}|_{2,h}. \tag{5.20}$$

From (5.19), (5.20) and Lemma 5.4 we have

$$\|w - w_\pi^\ell\|_{\mathrm{L}^2(\Gamma)} + h|w - w_\pi^\ell|_{h,1} \leq Ch^s \left(|w|_{\mathrm{H}^s(\Gamma)} + h|w|_{\mathrm{H}^1(\Gamma)}\right), \tag{5.21}$$

$$\|v - v_I^\ell\|_{\mathrm{L}^2(\Gamma)} + h|v - v_I^\ell|_{\mathrm{H}^1(\Gamma)} \leq Ch^2 \left(|v|_{\mathrm{H}^2(\Gamma)} + h|v|_{\mathrm{H}^1(\Gamma)}\right), \tag{5.22}$$

that are the desired estimates. □

The following Lemma generalises Lemma 4.7 in [37] to our polygonal/virtual setting and provides bounds for the geometric errors in the bilinear forms.

Lemma 5.6. *For any* $(v, w) \in \mathrm{H}^1(\Gamma_h) \times \mathrm{H}^1(\Gamma_h)$*, the following estimates hold:*

$$|\langle v^\ell, w^\ell \rangle_{\mathrm{L}^2(\Gamma)} - \langle v, w \rangle_{\mathrm{L}^2(\Gamma_h)}| \leq Ch^2 \|v^\ell\|_{\mathrm{L}^2(\Gamma)} \|w^\ell\|_{\mathrm{L}^2(\Gamma)}; \tag{5.23}$$

$$|a(v^\ell, w^\ell) - \bar{a}(v, w)| \leq Ch^2 \|\nabla_\Gamma v^\ell\|_{\mathrm{L}^2(\Gamma)} \|\nabla_\Gamma w^\ell\|_{\mathrm{L}^2(\Gamma)}, \tag{5.24}$$

where C *depends only on the geometry of* Γ*.*

Proof. We proceed as in Lemma 4.7 of [37], but here using, into (5.5)–(5.6), the generalised estimates (5.7)–(5.9) given in the previous Lemma 5.3. □

In the first section we have recalled the Poincaré inequality (2.9) in $\mathrm{H}_0^1(\Gamma)$. In the following theorem we prove an analogous inequality in $\mathrm{H}_0^1(\Gamma_h)$, *i.e.* on polygonal surfaces Γ_h of the type (4.1).

Theorem 5.7 (Poincaré inequality in $\mathrm{H}_0^1(\Gamma_h)$)**.** *Let* Γ *be a closed* C^2 *orientable surface in* $\mathbb{R}^3$*. Then there exist* $h_0 > 0$ *and* $C > 0$ *depending on* Γ *such that, for all* $0 < h < h_0$ *and* Γ_h *as in* (4.1)*,*

$$\|v\|_{\mathrm{L}^2(\Gamma_h)} \leq C|v|_{\mathrm{H}^1(\Gamma_h)} \qquad \forall v \in \mathrm{H}_0^1(\Gamma_h). \tag{5.25}$$

Proof. From (5.14) and the triangle inequality we have

$$\|v\|_{\mathrm{L}^2(\Gamma_h)} \leq C\|v^\ell\|_{\mathrm{L}^2(\Gamma)} \leq C\left(\left\|v^\ell - \frac{1}{|\Gamma|}\int_\Gamma v^\ell\right\|_{\mathrm{L}^2(\Gamma)} + \frac{1}{|\Gamma|^{\frac{1}{2}}}\int_\Gamma v^\ell\right). \tag{5.26}$$

Now, from (5.14) we have that $v^\ell - \frac{1}{|\Gamma|}\int_\Gamma v^\ell \in \mathrm{H}_0^1(\Gamma)$. Then, from Poincaré's inequality (2.9) and (5.15) it follows that

$$\left\|v^\ell - \frac{1}{|\Gamma|}\int_\Gamma v^\ell\right\|_{\mathrm{L}^2(\Gamma)} \leq C|v^\ell|_{\mathrm{H}^1(\Gamma)} \leq C|v|_{\mathrm{H}^1(\Gamma_h)}. \tag{5.27}$$

Furthermore, from (5.14), (5.23) and the fact that v is zero-averaged on Γ_h, it follows that

$$\frac{1}{|\Gamma|^{\frac{1}{2}}}\int_\Gamma v^\ell \leq \frac{1}{|\Gamma|^{\frac{1}{2}}}\left(\left|\int_{\Gamma_h} v\right| + Ch^2\|v^\ell\|_{\mathrm{L}^2(\Gamma)}|\Gamma|^{\frac{1}{2}}\right) \leq Ch^2\|v\|_{\mathrm{L}^2(\Gamma_h)}. \tag{5.28}$$

Combining (5.26), (5.27) and (5.28) we have

$$(1 - Ch^2)\|v\|_{\mathrm{L}^2(\Gamma_h)} \leq C|v|_{\mathrm{H}^1(\Gamma)}.$$

By choosing, for instance, $h_0 = \frac{1}{\sqrt{2C}}$, the result follows. □

Concerning the convergence rates of the above results we observe that:

- As shown in Lemma 5.6, in the approximation of the bilinear forms (5.23) and (5.24), the polygonal approximation of geometry yields a geometric error that is quadratic in L^2 norm and linear in H^1 norm. In fact, this Lemma is based on the geometric estimates of Lemma 5.3.
- The interpolation error on Γ, as shown by (5.17) in Lemma 5.5 (and its proof) arises from two sources. The first one is the interpolation error on flat polygons (cp. Lem. 5.1). The second one is given by the geometric estimates given in Lemma 5.3.

This implies that using higher-order virtual element spaces instead of (4.5) will not improve the convergence rate of the method, since geometric error would dominate over the interpolation one. The same drawback occurs with the standard SFEM [37] of higher order; in [45] it has been shown that a finite element space of degree $k \in \mathbb{N}$ defined on a suitable curvilinear triangulation of degree k (isoparametric elements) provides a SFEM with the same H^1 convergence rate as polynomial interpolation of degree k. This suggests that, to formulate a SVEM of order $k > 1$, a different approximation of the surface is needed.

We close this section proving an error estimate for the approximate right hand side $\langle f_h, v_h\rangle_h$ in the discrete formulation (4.25).

Theorem 5.8. *Let $f \in \mathrm{H}_0^1(\Gamma)$. Under the regularity assumptions (A1)–(A2), there exists $C > 0$ depending on Γ and γ such that*

$$|\langle f, v_h^\ell\rangle_{\mathrm{L}^2(\Gamma)} - \langle f_h, v_h\rangle_h| \leq Ch\left(|f|_{\mathrm{H}^1(\Gamma)} + h|f|_{\mathrm{H}^2(\Gamma)}\right)|v_h^\ell|_{\mathrm{H}^1(\Gamma)} \qquad \forall v_h \in W_h. \tag{5.29}$$

Proof. Let f_I be as in (4.10) and f_h be as in (4.25). We split the error as

$$\begin{aligned}|\langle f, v_h^\ell\rangle_{\mathrm{L}^2(\Gamma)} - \langle f_h, v_h\rangle_h| \leq{}& |\langle f, v_h^\ell\rangle_{\mathrm{L}^2(\Gamma)} - \langle f_I, v_h\rangle_{\mathrm{L}^2(\Gamma_h)}| + |\langle f_I, v_h\rangle_{\mathrm{L}^2(\Gamma_h)} - \langle f_h, v_h\rangle_{\mathrm{L}^2(\Gamma_h)}| \\ &+ |\langle f_h, v_h\rangle_{\mathrm{L}^2(\Gamma_h)} - \langle f_h, v_h\rangle_h|.\end{aligned} \tag{5.30}$$

From the Cauchy-Schwarz inequality (5.23) we obtain

$$\begin{aligned}|\langle f, v_h^\ell\rangle_{\mathrm{L}^2(\Gamma)} - \langle f_I, v_h\rangle_{\mathrm{L}^2(\Gamma_h)}| &\leq |\langle f - f_I^\ell, v_h^\ell\rangle_{\mathrm{L}^2(\Gamma)}| + |\langle f_I^\ell, v_h^\ell\rangle_{\mathrm{L}^2(\Gamma)} - \langle f_I, v_h\rangle_{\mathrm{L}^2(\Gamma_h)}| \\ &\leq \|f - f_I^\ell\|_{\mathrm{L}^2(\Gamma)}\|v_h^\ell\|_{\mathrm{L}^2(\Gamma)} + Ch^2\|f_I^\ell\|_{\mathrm{L}^2(\Gamma)}\|v_h^\ell\|_{\mathrm{L}^2(\Gamma_h)}.\end{aligned} \tag{5.31}$$

From the Cauchy-Schwarz inequality, the definition of f_h and (5.23) we have

$$\begin{aligned}
&|\langle f_I, v_h\rangle_{\mathrm{L}^2(\Gamma_h)} - \langle f_h, v_h\rangle_{\mathrm{L}^2(\Gamma_h)}| \le |\Gamma_h|^{-\frac{1}{2}} |\langle f_I, 1\rangle_{\mathrm{L}^2(\Gamma_h)}| \|v_h\|_{\mathrm{L}^2(\Gamma_h)} \\
&\le |\Gamma_h|^{-\frac{1}{2}} \left(|\langle f_I^\ell - f, 1\rangle_{\mathrm{L}^2(\Gamma)}| + Ch^2 \|f_I^\ell\|_{\mathrm{L}^2(\Gamma)} \right) \|v_h\|_{\mathrm{L}^2(\Gamma_h)} \\
&\le \left(\|f_I^\ell - f\|_{\mathrm{L}^2(\Gamma)} + Ch^2 \|f_I^\ell\|_{\mathrm{L}^2(\Gamma)} \right) \|v_h\|_{\mathrm{L}^2(\Gamma_h)}. \qquad (5.32)
\end{aligned}$$

Following [1], we know that

$$|\langle f_h, v_h\rangle_{\mathrm{L}^2(\Gamma_h)} - \langle f_h, v_h\rangle_h| \le Ch |f_h|_{1,h} |v_h|_{\mathrm{H}^1(\Gamma_h)}, \qquad (5.33)$$

but, from the definition of f_h and from (5.15) it follows that

$$|f_h|_{1,h} = |f_I|_{\mathrm{H}^1(\Gamma_h)} \le C |f_I^\ell|_{\mathrm{H}^1(\Gamma)}. \qquad (5.34)$$

Combining (5.30)–(5.34), using (5.14), (5.15), (5.17), the Poincaré inequalities (2.9), (5.25) and the triangle inequality we obtain

$$\begin{aligned}
&|\langle f, v_h^\ell\rangle_{\mathrm{L}^2(\Gamma)} - \langle f_h, v_h\rangle_h| \le \left(\|f - f_I^\ell\|_{\mathrm{L}^2(\Gamma)} + Ch |f_I^\ell|_{\mathrm{H}^1(\Gamma)} + Ch^2 \|f_I^\ell\|_{\mathrm{L}^2(\Gamma)} \right) |v_h^\ell|_{\mathrm{H}^1(\Gamma)} \\
&\le \left((1+Ch^2) \|f - f_I^\ell\|_{\mathrm{L}^2(\Gamma)} + Ch^2 \|f\|_{\mathrm{L}^2(\Gamma)} + Ch |f - f_I^\ell|_{\mathrm{H}^1(\Gamma)} + Ch |f|_{\mathrm{H}^1(\Gamma)} \right) |v_h^\ell|_{\mathrm{H}^1(\Gamma)} \\
&\le C \left((h^2 + h^4) |f|_{\mathrm{H}^2(\Gamma)} + (h + h^3 + h^5) |f|_{\mathrm{H}^1(\Gamma)} \right) |v_h^\ell|_{\mathrm{H}^1(\Gamma)} \le Ch \left(|f|_{\mathrm{H}^1(\Gamma)} + h |f|_{\mathrm{H}^2(\Gamma)} \right) |v_h^\ell|_{\mathrm{H}^1(\Gamma)},
\end{aligned}$$

that is the desired estimate. □

6. Existence, uniqueness and error analysis

The following theorem, that is the main result of this paper, extends Theorem 3.1 in [1] for the VEM on planar domains to the Laplace-Beltrami equation on surfaces. In fact, it provides: (i) the existence and the uniqueness of the solution for both the continuous (3.3) and the discrete problem (4.25) and (ii) an abstract convergence result. As a corollary, an optimal $\mathrm{H}^1(\Gamma)$ error estimate for problem (4.25) will be given.

Theorem 6.1 (Abstract convergence theorem)**.** *Let $a : \mathrm{H}_0^1(\Gamma) \times \mathrm{H}_0^1(\Gamma) \to \mathbb{R}$ be the bilinear form defined by*

$$a(u,v) = \int_\Gamma \nabla_\Gamma u \cdot \nabla_\Gamma v \qquad \forall u, v \in \mathrm{H}_0^1(\Gamma),$$

and let $a_h : W_h \times W_h \to \mathbb{R}$ be any symmetric bilinear form such that

$$a_h(u_h, v_h) = \sum_{E \in \mathcal{T}_h} a_{h,E}(u_{h|E}, v_{h|E}), \qquad (6.1)$$

where, for all $E \in \mathcal{T}_h$, $a_{h,E}$ is a symmetric bilinear form on $V_h(E) \times V_h(E)$ such that

$$|a_{h,E}(p, v_{h,E}) - a_{\tilde{E}}(p^\ell, v_{h,E}^\ell)| \le Ch^2 |p^\ell|_{\mathrm{H}^1(\tilde{E})} |v_{h,E}^\ell|_{\mathrm{H}^1(\tilde{E})} \qquad \forall v_{h,E} \in V_h(E),\ \forall p \in \mathbb{P}_1(E); \qquad (6.2)$$

$$\alpha_* a_{\tilde{E}}(v_{h,E}^\ell, v_{h,E}^\ell) \le a_{h,E}(v_{h,E}, v_{h,E}) \le \alpha^* a_{\tilde{E}}(v_{h,E}^\ell, v_{h,E}^\ell) \qquad \forall v_{h,E} \in V_h(E), \qquad (6.3)$$

where α_* and α^* are independent of h and $E \in \mathcal{T}_h$.

Let $F \in \mathrm{L}^2(\Gamma)'$ and $F_h \in W_h'$ be linear continuous functionals. Consider the problems

$$\begin{cases} u \in \mathrm{H}_0^1(\Gamma) \\ a(u,v) = F(v) \quad \forall v \in \mathrm{H}_0^1(\Gamma) \end{cases} \qquad (6.4)$$

$$\begin{cases} u_h \in W_h \\ a_h(u_h, v_h) = F_h(v_h) \quad \forall v_h \in W_h \end{cases} \qquad (6.5)$$

Both of these problems have a unique solution and the following error estimate holds

$$|u-u_h^\ell|_{\mathrm{H}^1(\Gamma)} \le C\left(|u-u_\pi^\ell|_{h,1}+|u-u_I^\ell|_{\mathrm{H}^1(\Gamma)}+\mathcal{F}_h+h\|F\|_{\mathrm{L}^2(\Gamma)'}\right), \tag{6.6}$$

where $\mathcal{F}_h$ is the smallest constant such that

$$|F(v_h^\ell)-F_h(v_h)| \le \mathcal{F}_h|v_h^\ell|_{\mathrm{H}^1(\Gamma)} \qquad \forall v_h\in W_h. \tag{6.7}$$

Proof. Existence and uniqueness follow from Lax-Milgram's theorem. In fact, from the Poincaré inequality (2.9) on $\mathrm{H}^1_0(\Gamma)$, the bilinear form a is coercive and, from the Cauchy-Schwarz inequality, it is continuous. The bilinear form a_h is coercive since

$$\begin{aligned}|a_h(v_h,v_h)| &\underset{(6.1)}{=} \left|\sum_{E\in\mathcal{T}_h} a_{h,E}(v_{h|E},v_{h|E})\right| \underset{(6.3)}{\ge} \alpha_* \sum_{E\in\mathcal{T}_h}\left|a_{\tilde{E}}(v_{h|E}^\ell,v_{h|E}^\ell)\right| = \alpha_*\sum_{E\in\mathcal{T}_h}|v_h^\ell|^2_{\mathrm{H}^1(\tilde{E})}\\ &\underset{(5.15)}{\ge} C\sum_{E\in\mathcal{T}_h}|v_h|^2_{\mathrm{H}^1(E)} = C|v_h|^2_{\mathrm{H}^1(\Gamma_h)} \underset{(5.25)}{\ge} C\|v_h\|^2_{\mathrm{H}^1(\Gamma_h)},\end{aligned}$$

for all $v_h\in W_h$. Now we prove that a_h is continuous. To this end, since a_h is symmetric and coercive (*i.e.* positive definite), then it fulfills the Cauchy-Schwarz inequality. Then we have

$$\begin{aligned}|a_h(v_h,w_h)| &\underset{(6.1)}{\le} \sum_{E\in\mathcal{T}_h}|a_{h,E}(v_{h|E},w_{h|E})| \le \sum_{E\in\mathcal{T}_h} a_{h,E}(v_{h|E},v_{h|E})^{\frac12}a_{h,E}(w_{h|E},w_{h|E})^{\frac12}\\ &\underset{(6.3)}{\le} \alpha^*\sum_{E\in\mathcal{T}_h} a_{\tilde{E}}(v_{h|E}^\ell,v_{h|E}^\ell)^{\frac12}a_{\tilde{E}}(w_{h|E}^\ell,w_{h|E}^\ell)^{\frac12} = \alpha^*\sum_{E\in\mathcal{T}_h}|v_h^\ell|_{\mathrm{H}^1(\tilde{E})}|w_h^\ell|_{\mathrm{H}^1(\tilde{E})} \underset{(5.15)}{\le} C\sum_{E\in\mathcal{T}_h}|v_h|_{\mathrm{H}^1(E)}|w_h|_{\mathrm{H}^1(E)}\\ &\le C\left(\sum_{E\in\mathcal{T}_h}|v_h|^2_{\mathrm{H}^1(E)}\right)^{\frac12}\left(\sum_{E\in\mathcal{T}_h}|w_h|^2_{\mathrm{H}^1(E)}\right)^{\frac12} = C|v_h|_{\mathrm{H}^1(\Gamma_h)}|w_h|_{\mathrm{H}^1(\Gamma_h)} \le C\|v_h\|_{\mathrm{H}^1(\Gamma_h)}\|w_h\|_{\mathrm{H}^1(\Gamma_h)},\end{aligned}$$

for all $v_h,w_h\in W_h$. Hence, problems (6.4) and (6.5) meet the assumptions of Lax-Milgram's theorem.

If $\mathbf{a}:\Gamma_h\to\Gamma$ is the projection onto Γ defined in (2.2), then for any $E\in\mathcal{T}_h$, let $\tilde{E}=\mathbf{a}(E)$ be the curved element corresponding to E. Let $u_\pi\in\prod_{E\in\mathcal{T}_h}\mathbb{P}_1(E)$ be the projection of u defined in (5.18) and let $u_I\in W_h$ be the interpolant of u defined in (5.17). From [37, Theorem 3.3], The solution of (6.4) fulfills $u\in\mathrm{H}^2(\Gamma)$ and thus u_π and u_I are well-defined. Let $\delta_h=u_h-u_I$. It holds that

$$\begin{aligned}&\alpha_*|\delta_h^\ell|^2_W = \alpha_* a(\delta_h^\ell,\delta_h^\ell) \le a_h(\delta_h,\delta_h) = a_h(u_h,\delta_h)-a_h(u_I,\delta_h)\\ &\underset{(6.1)}{=} F_h(\delta_h)-\sum_{E\in\mathcal{T}_h}a_{h,E}(u_I,\delta_h) = F_h(\delta_h)-\sum_{E\in\mathcal{T}_h}\left(a_{h,E}(u_I-u_\pi,\delta_h)+a_{h,E}(u_\pi,\delta_h)\right)\\ &\underset{(6.2)}{\le} F_h(\delta_h)-\sum_{E\in\mathcal{T}_h}\left(a_{h,E}(u_I-u_\pi,\delta_h)+a_{\tilde{E}}(u_\pi^\ell,\delta_h^\ell)\right)+Ch^2\sum_{E\in\mathcal{T}_h}|u_\pi^\ell|_{\mathrm{H}^1(\tilde{E})}|\delta_h^\ell|_{\mathrm{H}^1(\tilde{E})}\\ &= F_h(\delta_h)-\sum_{E\in\mathcal{T}_h}\left(a_{h,E}(u_I-u_\pi,\delta_h)+a_{\tilde{E}}(u_\pi^\ell-u,\delta_h^\ell)+a_{\tilde{E}}(u,\delta_h^\ell)\right)+Ch^2\left(|u_\pi^\ell|^2_{h,1}+|\delta_h^\ell|^2_{\mathrm{H}^1(\Gamma)}\right)\\ &= F_h(\delta_h)-a(u,\delta_h^\ell)-\sum_{E\in\mathcal{T}_h}\left(a_{h,E}(u_I-u_\pi,\delta_h)+a_{\tilde{E}}(u_\pi^\ell-u,\delta_h^\ell)\right)+Ch^2\left(|u_\pi^\ell|^2_{h,1}+|\delta_h^\ell|^2_{\mathrm{H}^1(\Gamma)}\right)\\ &= F_h(\delta_h)-F(\delta_h^\ell)-\sum_{E\in\mathcal{T}_h}\left(a_{h,E}(u_I-u_\pi,\delta_h)+a_{\tilde{E}}(u_\pi^\ell-u,\delta_h^\ell)\right)+Ch^2\left(|u_\pi^\ell|^2_{h,1}+|\delta_h^\ell|^2_{\mathrm{H}^1(\Gamma)}\right).\end{aligned}$$

From (6.3), (6.7) and the continuity of a and a_h we obtain

$$(\alpha_*-Ch^2)|\delta_h^\ell|^2_{\mathrm{H}^1(\Gamma)} \le \mathcal{F}_h|\delta_h^\ell|_{\mathrm{H}^1(\Gamma)}+|u_I-u_\pi|_{h,1}|\delta_h|_{\mathrm{H}^1(\Gamma_h)}+|u_\pi^\ell-u|_{h,1}|\delta_h^\ell|_{\mathrm{H}^1(\Gamma)}+Ch^2|u_\pi^\ell|^2_{h,1}.$$

For h sufficiently small, by exploiting (5.15), we obtain

$$|\delta_h^\ell|^2_{\mathrm{H}^1(\Gamma)} \leq C(\mathcal{F}_h + |u_I^\ell - u_\pi^\ell|_{h,1} + |u_\pi^\ell - u|_{h,1})|\delta_h^\ell|_{\mathrm{H}^1(\Gamma)} + Ch^2|u_\pi^\ell|^2_{h,1}. \tag{6.8}$$

By defining $A = \mathcal{F}_h + |u_I^\ell - u_\pi^\ell|_{h,1} + |u_\pi^\ell - u|_{h,1}$ and solving the second-degree-algebraic inequality (6.8) we have

$$|\delta_h^\ell|_{\mathrm{H}^1(\Gamma)} \leq \frac{CA}{2} + \frac{1}{2}\sqrt{C^2A^2 + 4Ch^2|u_\pi^\ell|^2_{h,1}} \leq \frac{CA}{2} + \frac{1}{2}(CA + 2\sqrt{C}h|u_\pi^\ell|_{h,1}) \leq CA + Ch|u_\pi^\ell|_{h,1}.$$

By recalling the definition of A and applying the triangle inequality, we get

$$|u - u_h^\ell|_{\mathrm{H}^1(\Gamma)} \leq C(\mathcal{F}_h + |u - u_I^\ell|_{\mathrm{H}^1(\Gamma)} + |u - u_\pi^\ell|_{h,1}) + Ch|u_\pi^\ell|_{h,1}.$$

By applying the triangle inequality to the last term, we obtain

$$|u - u_h^\ell|_{\mathrm{H}^1(\Gamma)} \leq C\left(\mathcal{F}_h + |u - u_I^\ell|_{\mathrm{H}^1(\Gamma)} + (1+h)|u - u_\pi^\ell|_{h,1} + h|u|_{\mathrm{H}^1(\Gamma)}\right).$$

The obvious stability estimate $|u|_{\mathrm{H}^1(\Gamma)} \leq C\|F\|_{\mathrm{L}^2(\Gamma)'}$, where C is the constant in the Poincaré inequality (2.9), together with $h \leq h_0$, complete the proof. □

From the abstract framework given in Theorem 6.1 we are now ready to derive the $\mathrm{H}^1(\Gamma)$ error estimate between the continuous problem (3.3) and the discrete one (4.25).

Corollary 6.2 ($\mathrm{H}^1(\Gamma)$ error estimate)**.** *Problems* (3.3) *and* (4.25) *have a unique solution. Let u and u_h be the their solutions, respectively. Under the mesh regularity assumptions (A1)–(A2), if $f \in \mathrm{H}^2_0(\Gamma)$, the following estimate holds:*

$$|u - u_h^\ell|_{\mathrm{H}^1(\Gamma)} \leq Ch(|u|_{\mathrm{H}^2(\Gamma)} + |f|_{\mathrm{H}^1(\Gamma)}) + Ch^2|f|_{\mathrm{H}^2(\Gamma)}. \tag{6.9}$$

Proof. In Theorem 6.1, we choose

$$\begin{aligned} F(v) &= \langle f, v\rangle_{\mathrm{L}^2(\Gamma)} \qquad \forall v \in \mathrm{H}^1(\Gamma);\\ F_h(v_h) &= \langle f_h, v_h\rangle_h \qquad \forall v_h \in W_h, \end{aligned}$$

with a_h defined in (4.11), (4.15). Under the regularity assumptions (A1)–(A2),

(1) Assumption (6.2) follows from (4.14) and (5.24);
(2) Assumption (6.3) follows from (4.11), (4.13) and (5.15);
(3) From [37, Theorem 3.3] we have $u \in \mathrm{H}^2(\Gamma)$. Then, Theorem 5.5 provides

$$|u - u_\pi^\ell|_{h,1} + |u - u_I^\ell|_{\mathrm{H}^1(\Gamma)} < Ch(|u|_{\mathrm{H}^2(\Gamma)} + h|u|_{\mathrm{H}^1(\Gamma)}); \tag{6.10}$$

(4) if $f \in \mathrm{H}^1_0(\Gamma)$, the Poincaré inequality (2.9) provides

$$\|F\|_{\mathrm{L}^2(\Gamma)'} = \|f\|_{\mathrm{L}^2(\Gamma)} \leq C|f|_{\mathrm{H}^1(\Gamma)}, \tag{6.11}$$

and (5.29) yields

$$\mathcal{F}_h \leq Ch(|f|_{\mathrm{H}^1(\Gamma)} + h|f|_{\mathrm{H}^2(\Gamma)}). \tag{6.12}$$

By plugging (6.10)–(6.12), into the abstract error bound (6.6), we obtain

$$|u - u_h^\ell|_{\mathrm{H}^1(\Gamma)} \leq Ch(|u|_{\mathrm{H}^2(\Gamma)} + |f|_{\mathrm{H}^1(\Gamma)}) + Ch^2(|u|_{\mathrm{H}^1(\Gamma)} + |f|_{\mathrm{H}^2(\Gamma)}). \tag{6.13}$$

By plugging the Poincaré inequality (2.9), the stability estimate $|u|_{\mathrm{H}^1(\Gamma)} \leq C\|F\|_{\mathrm{L}^2(\Gamma)'}$ and (6.11) into (6.13), the result follows. □

7. Implementation

In this section we will discuss how to implement the SVEM using only information on the mesh and the nodal values of the load term f. The major differences with respect to the planar case are:

(1) construction of test problems on arbitrary surfaces, with the knowledge of the exact solution and construction of polygonal meshes;
(2) computation of local matrices (mass, stiffness and load term);
(3) formulation of the discrete problem as a square, full-rank linear system which also accounts for the zero-average condition on the solution.

7.1. Constructing test problems

To perform a convergence study of any numerical method for the Laplace-Beltrami equation, it is necessary to construct some *test problems*, where the exact solution is known in closed form. Constructing test problems, which is trivial in the planar case, is more involved on curved surfaces. For a generic surface, we proceed as follows:

Represent Γ as a zero level set of a suitable function ϕ as in Definition 2.1;
(1) Compute the unit normal vector field ν according to (2.1);
(2) Choose the exact solution u such that u is well-defined and sufficiently smooth in an open neighbourhood of Γ;
(3) By repeatedly computing the tangential derivatives of u as in (2.4), compute the Laplace-Beltrami of u according to (2.5), thus obtaining the right-hand side f of the Laplace-Beltrami equation (3.1). We remark that, if Γ has no boundary, then, by construction, f is zero-averaged on Γ.

Though being merely algorithmic, this procedure can be particularly lengthy and tedious even on rather simple surfaces, neverthless a symbolic calculus software could be used for this task.

On very special surfaces, such as spheres and cylinders, some eigenfunctions of the Laplace-Beltrami operator are known in the literature [46]. Hence, if $\bar{u}$ is an eigenfunction of $-\Delta_\Gamma$ with eigenvalue λ, a test problem is immediately obtained by choosing the load term as $f = \lambda\bar{u}$. This approach will be used in our numerical example provided in next Section 8 (Experiment 8.2.1).

Concerning the discretisation of generic surfaces for a Laplace-Beltrami equation, to the best of the author's knowledge, the problem of generating and refining arbitrary polygonal meshes is an open question and no general algorithm is available. More is known on the specific case of triangular meshes, see [37, 47, 48] and some codes are available [49, 50]. Here we suggest a possible way of constructing polygonal meshes in the following cases:

(1) On spherical surfaces: polygonal meshes can be constructed starting from arbitrary triangulations by suitably subdiving the triangles and projecting the resulting nodes onto Γ, as explained in Figure 3 for a single triangle. In the caption of this figure we describe the steps required by this construction. We will apply this approach in Experiment 8.2.1, see Figure 6a. Steps of the construction are explained in the caption of Figure 3.
(2) For special surfaces, such as cylinders or tori: it is possible to trivially construct quadrilateral or trapezoidal meshes that significantly reduce the number of elements, on equal number of degrees of freedom. We will consider these meshes in Experiments 8.2.2 and 8.2.3.

7.2. Constructing local matrices

In this section we explain how the construction of the stiffness and mass matrices on polygonal meshes in $\mathbb{R}^3$ differ from the planar case. Let $N \in \mathbb{N}$ be the number of vertices, say $\{\mathbf{x}_i,\ i = 1, \dots, N\}$, and for every $i = 1, \dots, N$ let $\phi_i \in V_h$ be the i-th basis function defined by $\phi_i(\mathbf{x}_j) = \delta_{ij}$, for all $j = 1, \dots, N$. For every

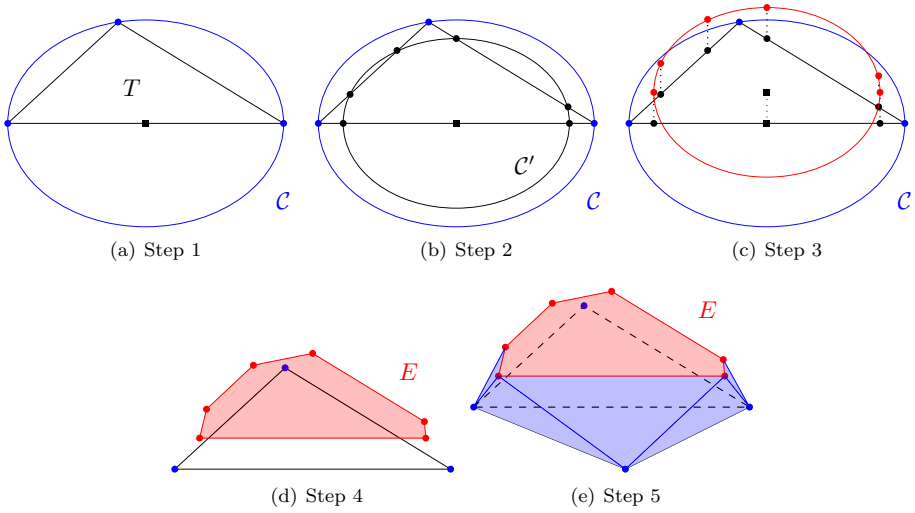

(a) Step 1 (b) Step 2 (c) Step 3

(d) Step 4 (e) Step 5

FIGURE 3. Generating a polygonal mesh on the sphere. (a) Given a triangular element T, we consider the out-circle $\mathcal{C}$ (which is contained in Γ). (b) We consider a circle $\mathcal{C}'$, concentric with $\mathcal{C}'$, whose radius is such that $\mathcal{C}'$ intersect each edge of T in two distinct points. (c) The resulting six points are moved, orthogonally to the plane of T, onto Γ. (d) By connecting these points, an hexagon E is created, whose vertices are on Γ. (e) New triangles are added to connect the nodes of E with the neighboring nodes of T.

element $E \in \mathcal{T}_h$, consider the local mass and stiffness matrices M_E and A_E defined respectively by

$$M_E = (m_{ij}^E) := \langle \phi_i, \phi_j \rangle_{\mathrm{L}^2_h, E} \qquad \forall i, j : \mathbf{x}_i, \mathbf{x}_j \in \mathrm{nodes}(E);$$
$$A_E = (a_{ij}^E) := a_{h,E}(\phi_i, \phi_j) \qquad \forall i, j : \mathbf{x}_i, \mathbf{x}_j \in \mathrm{nodes}(E).$$

For all $E \in \mathcal{T}_h$, we move E to the horizontal plane $\{z = 0\}$ and we use the algorithm described in [8] for the computation of the local matrices in the planar case.

To move E onto the horizontal plane, we proceed as follows. Let $n_E \in \mathbb{N}$ be the number of vertices of E, let P_i, $i = 1, \dots, n_E$ be the vertices of E and let $P_i' = (x_i', y_i')$, $i = 1, \dots, n_E$, be the vertices of the transformed element. For the sake of simpleness, we fix the transformation by enforcing that

(1) the first vertex P_1 is moved to the origin, *i.e.* $P_1' = O$;
(2) the second vertex P_2 is moved onto the x-axis, *i.e.* $y_2' = 0$;
(3) if $j := \min\{i = 3, \dots, n_E \mid P_1, P_2 \text{ and } P_j \text{ are not aligned}\}$, then P_j is moved onto the positive y half-plane, *i.e.* $y_j' > 0$.

The vertices of the transformed element can be computed with the following rule:

$$x_1' = 0, \qquad x_i' = \frac{(P_2 - P_1) \cdot (P_i - P_1)}{\|P_2 - P_1\|}, \qquad i = 2, \dots, n_E;$$
$$y_1' = y_2' = 0, \qquad |y_i'| = \frac{\|(P_2 - P_1) \times (P_i - P_1)\|}{\|P_2 - P_1\|}, \qquad i = 3, \dots, n_E;$$
$$y_j' > 0, \qquad \operatorname{sign} y_i' = \operatorname{sign}\left((P_2 - P_1) \times (P_j - P_1)\right) \cdot \left((P_2 - P_1) \times (P_i - P_1)\right), \qquad i = j+1, \dots, n_E,$$

where $\times$ denotes the cross-product. Notice that the transformed elements are used in the computation of the local matrices, only. The numerical solution is then plotted on the original mesh in $\mathbb{R}^3$.

7.3. Full-rank linear system associated to SVEM for the Laplace-Beltrami equation

As pointed out in Remark 3.1, the Laplace-Beltrami equation must be complemented with the zero-average condition when (i) Γ has no boundary or (ii) The boundary condition are of homogeneous Neumann type. In this subsection we explain how to write the discrete formulation as a square, full-rank linear system that accounts for the zero-average condition and whose dimension is minimal, *i.e.* equal to the number of vertices. To this end, we observe that, from (4.9) and (4.24), problem (4.25) is equivalent to

$$\begin{cases} u_h \in V_h \\ a_h(u_h, \phi_h) = \langle f_h, \phi_h \rangle_h \qquad \forall\ \phi_h \in V_h \\ \langle u_h, 1 \rangle_{\mathrm{L}^2(\Gamma_h)} = 0. \end{cases} \tag{7.1}$$

Notice that the overall number of degrees of freedom is equal to the number N of nodal points. We express the numerical solution of (7.1) in the basis $\{\phi_i\}_{i=1}^N$ as

$$u_h(\mathbf{x}) = \sum_{j=1}^{N} \xi_j \phi_j(\mathbf{x}) \qquad \forall \mathbf{x} \in \Gamma_h,$$

with $\xi_j \in \mathbb{R}$ for all $j = 1, \dots, N$. Problem (4.25) is then equivalent to

$$\sum_{j=1}^{N} a_h(\phi_i, \phi_j)\xi_j = \langle f_h, \phi_i \rangle_h \qquad \forall i = 1, \dots, N, \tag{7.2}$$

$$\sum_{j=1}^{N} \langle 1, \phi_j \rangle_{\mathrm{L}_h^2} \xi_j = 0. \tag{7.3}$$

Problem (7.2)–(7.3) is a rectangular $(N+1) \times N$ linear system that has, from Corollary 6.2, a unique solution. We want to rephrase this problem as a square $N \times N$ linear system. To this end, notice that the function $\bar{\phi} := \sum_{i=1}^N \phi_i$ fulfils $\bar{\phi}(\mathbf{x}_j) = 1$ for all $j = 1, \dots, N$ and thus, from (4.5), we have

$$\sum_{i=1}^{N} \phi_i(\mathbf{x}) = 1 \qquad \forall \mathbf{x} \in \Gamma_h. \tag{7.4}$$

We show that the sum of all equations in (7.2) vanishes. In fact, for the left hand side of (7.2), using (4.14) and (7.4), we have that

$$\sum_{i=1}^{N}\sum_{j=1}^{N} a_h(\phi_i, \phi_j)\xi_j = \sum_{j=1}^{N} a_h\left(\sum_{i=1}^{N} \phi_i, \phi_j\right)\xi_j = \sum_{j=1}^{N} a_h(1, \phi_j)\xi_j = \sum_{j=1}^{N} \bar{a}(1, \phi_j)\xi_j = 0,$$

while for the right hand side of (7.2), from (4.24) and (7.4) we have $\sum_{i=1}^N \langle f_h, \phi_i \rangle_h = \langle f_h, 1 \rangle_h = 0$. We conclude that the sum of equations (7.2) vanishes. This implies that we can remove, for instance, the N-th equation in (7.2). System (7.2)–(7.3) is then equivalent to the $N \times N$ system

$$\begin{cases} \displaystyle\sum_{j=1}^{N} a_h(\phi_i, \phi_j)\xi_j = \langle f_h, \phi_i \rangle_h \qquad \forall i = 1, \dots, N-1, \\ \displaystyle\sum_{j=1}^{N} \langle 1, \phi_j \rangle_{\mathrm{L}_h^2} \xi_j = 0. \end{cases}$$

Consider the stiffness matrix A, the mass matrix M, and the load term $\mathbf{b}$ defined by

$$A = (a_{ij}) := a_h(\phi_i, \phi_j), \quad M = (m_{ij}) := \langle \phi_i, \phi_j \rangle_{\mathrm{L}^2_h} \quad \forall i, j = 1, \dots, N, \qquad \mathbf{b} = (b_i) := \langle f_h, \phi_i \rangle_h \quad \forall i = 1, \dots, N.$$

The matrices A and M are assembled from the corresponding local matrices introduced in the previous section. To compute the load vector $\mathbf{b}$ we observe that, from (4.21) and the definition of the basis functions, it holds that

$$b_i = \sum_{E : \mathbf{x}_i \in \mathrm{nodes}(E)} \frac{1}{n_E} \int_E f_h \qquad \forall i = 1, \dots, N. \tag{7.5}$$

Each integral in (7.5) is computed as follows. The nodal values of the load term f_h are computed by

$$f_h(\mathbf{x}_k) = f_I(\mathbf{x}_k) - \frac{\langle f_I, 1 \rangle_{\mathrm{L}^2_h}}{|\Gamma_h|} = f(\mathbf{x}_k) - \frac{\sum_{i=1}^N \langle \phi_i, 1 \rangle_{\mathrm{L}^2_h} f(\mathbf{x}_i)}{\langle 1, 1 \rangle_{\mathrm{L}^2_h}} = f(\mathbf{x}_k) - \frac{\sum_{i=1}^N (\sum_{j=1}^N m_{ij}) f(\mathbf{x}_i)}{\sum_{i=1}^N \sum_{j=1}^N m_{ij}},$$

for all $k = 1, \dots, N$. For every E, the integral of f_h on E is given by

$$\int_E f_h \underset{(4.18)}{=} \langle f_h, 1 \rangle_{\mathrm{L}^2_h, E} = \sum_{i : \mathbf{x}_i \in \mathrm{nodes}(E)} \langle \phi_I, 1 \rangle_{\mathrm{L}^2_h, E} f_h(\mathbf{x}_i) = \sum_{i : \mathbf{x}_i \in \mathrm{nodes}(E)} \left(\sum_{j : \mathbf{x}_j \in \mathrm{nodes}(E)} m_{ij}^E \right) f_h(\mathbf{x}_i).$$

In conclusion, the discretisation of the Laplace-Beltrami equation (3.2) by SVEM is given by the following sparse, square, full-rank linear algebraic system

$$\begin{cases} \displaystyle\sum_{j=1}^N a_{ij} \xi_j = b_i \qquad \forall i = 1, \dots, N-1, \\ \displaystyle\sum_{j=1}^N \left(\sum_{i=1}^N m_{ij} \right) \xi_j = 0. \end{cases} \tag{7.6}$$

8. Applications and numerical examples

8.1. Mesh pasting

In this section we discuss a possible advantage of SVEM with respect to SFEM. Suppose that Γ is made up of two surfaces Γ_1 and Γ_2, joining along a curve ℓ, *i.e.* $\Gamma = \Gamma_1 \cup \Gamma_2$ and $\Gamma_1 \cap \Gamma_2 = \ell$. Furthermore, suppose we are given two corresponding polygonal surfaces $\Gamma_{1,h}$, $\Gamma_{2,h}$. We want to construct a polygonal surface Γ_h by pasting $\Gamma_{h,1}$ and $\Gamma_{h,2}$. Such a process can lead to nonconforming and/or discontinuous meshes. For this reason, pasting algorithms for standard FEMs typically need additional steps to deform the meshes and match the nodes, see for instance [12, 13]. As illustrated below, mesh pasting becomes trivial in the framework of the SVEM. We distinguish two cases.

Pasting along a straight line. In the first case ℓ is a straight line. Suppose that $\Gamma_{1,h}$ and $\Gamma_{2,h}$ are triangulations that fit ℓ exactly, *i.e.* $\Gamma_{1,h} \cap \Gamma_{2,h} = \ell$. An example of pasting process is depicted in Figure 4. As shown in Figure 4b this can lead, in general, to a nonconforming overall triangulation, that is Γ_h is composed of three quadrilaterals and two triangles in this specific example. It is well-known that the triangular FEMs, including SFEM, are not applicable to nonconforming meshes, since the basis functions are not well-defined in the presence of arbitrarily many vertices per polygon.

Pasting along an arbitrary curve. The general case when ℓ is an arbitrary curve is more interesting. In this case it is not true that $\Gamma_{1,h} \cap \Gamma_{2,h} = \ell$. In general, only the vertices of $\Gamma_{1,h}$ and $\Gamma_{2,h}$ lie on ℓ. Hence, $\Gamma_{h,1} \cup \Gamma_{h,2}$ might be a discontinuous mesh, as depicted in Figure 5b.

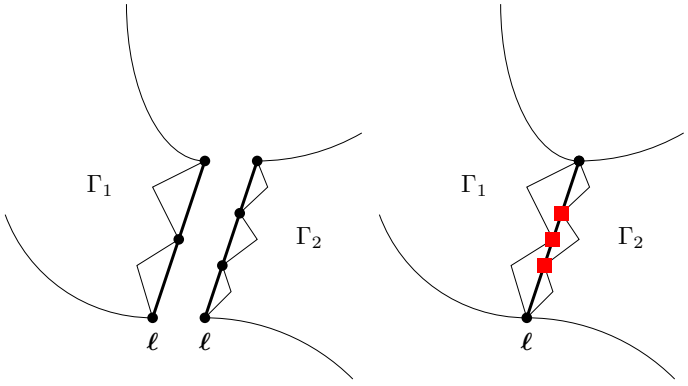

(a) Step 1 (b) Step 2

FIGURE 4. Pasting meshes along a straight line. Step 1: two surfaces Γ_1 and Γ_2 are given together with their approximations $\Gamma_{1,h}$ and $\Gamma_{2,h}$. The elements having an edge on ℓ are depicted and their nodes on ℓ are black-marked. Step 2: by pasting the polygonal surfaces, a nonconforming polygonation of $\Gamma = \Gamma_1 \cup \Gamma_2$ is formed, due to the presence of hanging nodes on ℓ, which are red-marked.

In order to apply the SVEM in this case, we proceed as follows:

(1) We sort the boundary nodes (*i.e.* that are on ℓ) of $\Gamma_{h,1} \cup \Gamma_{h,2}$ according to their curvilinear abscissa;
(2) For each pair (P, R) of subsequent boundary nodes of $\Gamma_{h,1}$, let T_1 be the element to which it belongs, see Figure 5a
(3) For any boundary node Q of the other polygonal surface $\Gamma_{h,2}$ that is between P and R, consider the orthogonal projection Q' of Q onto the edge $\overline{PR}$, as shown in Figure 5b;
(4) Add Q' to the element T_1 as a hanging node;
(5) Repeat steps (2)–(4) on the boundary nodes of the other mesh $\Gamma_{h,2}$;
(6) For any pair (Q, Q') as above, enforce the *virtual continuity* condition $u_h(Q) = u_h(Q')$ on the numerical solution u_h.

Note that if $Q = Q'$, then of course the continuity condition is automatically fulfilled, but a new nonconforming element arises (see *e.g.* $R = R'$ in Fig. 5b). We remark that, when assembling the matrices involved in the method (mass, stiffness and load term), Q and Q' are associated to the same degree of freedom, hence *virtual continuity* does not affect the size of the linear system associated to the SVEM. Once again, this procedure strongly relies on the possibility of handling polygons with arbitrarily many vertices and hanging nodes, where standard FEMs are not well-defined. Furthermore, we point out that our convergence analysis in Section 6 does not cover this case of discontinuous meshes. However, without giving full details, our analysis can be extended to the present case in a straightforward way. In fact, based on interpolation estimates, it can be proven that the distance $\|Q - Q'\|$ decays quadratically with the meshsize (a similar result has been proven in [51] in the planar case). In 8.2.3 we experimentally show that this approach to mesh pasting does not affect the convergence rate of the method.

8.2. Numerical tests

In this section we will validate the theoretical findings through numerical experiments.

In Experiment 1, a Laplace-Beltrami problem on the unit sphere, approximated with a polygonal mesh, is used to test the convergence rate in (6.9). The experiment also shows the robustness of the method with respect to "badly shaped" meshes, i.e with polygons of very different size and very tight, thus confirming the generality of assumptions (A1)–(A2). In Experiment 8.2.2, we solve the Laplace-Beltrami equation on a torus using the

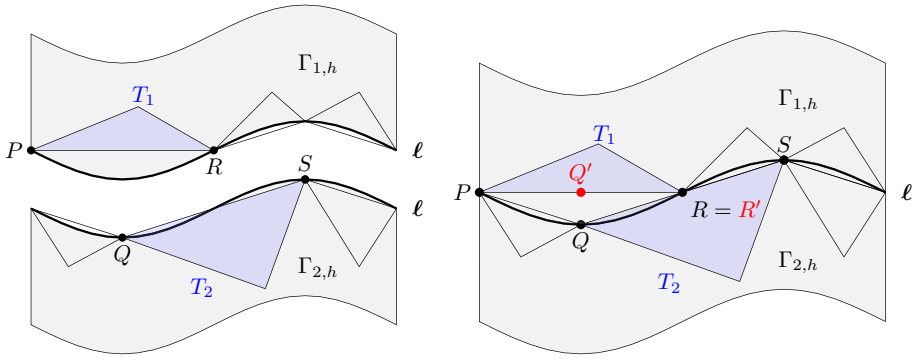

(a) Step 1 (b) Step 2

FIGURE 5. Pasting meshes along an arbitrary curve. (a) Step 1: two surfaces Γ_1 and Γ_2 are given together with their approximations $\Gamma_{1,h}$ and $\Gamma_{2,h}$. The elements having an edge on ℓ are depicted and some nodes on ℓ are black-marked. (b) Step 2: by pasting the polygonal surfaces, a discontinuous polygonation of $\Gamma = \Gamma_1 \cup \Gamma_2$ is formed. The new node Q' is obtained by projecting Q onto the edge $\overline{PR}$, so that the triangle T_1 becomes a quadrilateral with a hanging node, and the *virtual continuity* condition $u_h(Q) = u_h(Q')$ is enforced on the numerical solution. The node R coincides with its projection R' onto $\overline{QS}$ and the triangle T_2 becomes a quadrilateral with a hanging node.

SVEM on trapezoidal meshes. In Experiment 8.2.3, to present an example of mesh pasting along a curve, we solve the Laplace-Beltrami equation on a cylindrical surface. We show that, even if discontinuous meshes are used, the theoretical convergence order of the SVEM is preserved.

8.2.1. Experiment 1 (Sphere)

In this experiment we solve the Laplace-Beltrami equation

$$\begin{cases} -\Delta_\Gamma u(x,y,z) = 6xy, & (x,y,z) \in \Gamma, \\ \int_\Gamma u(x,y,z)\,\mathrm{d}\sigma = 0, \end{cases} \tag{8.1}$$

on the unit sphere $\Gamma := \mathcal{S}^2$, whose exact solution is given by $u(x,y,z) = xy$, $(x,y,z) \in \Gamma$. In this case, the Fermi stripe of Γ is $U = \mathbb{R}^3 \setminus \{\mathbf{0}\}$, the oriented distance function is given by $d(\mathbf{x}) = \|\mathbf{x}\| - 1$, $\mathbf{x} \in U$ and the outward unit normal vector field is given by $\nu(\mathbf{x}) = \mathbf{x}$, $\mathbf{x} \in \Gamma$. Hence, the representation (2.3) of the tangential gradient of a function $f \in \mathrm{C}^1(\Gamma)$ becomes

$$\nabla_\Gamma f(\mathbf{x}) = \nabla f(\mathbf{x}) - (\nabla f(\mathbf{x}) \cdot \mathbf{x})\mathbf{x} = \begin{bmatrix} 1-x^2 & -xy & -xz \\ -xy & 1-y^2 & -yz \\ -xz & -yz & 1-z^2 \end{bmatrix} \nabla f(\mathbf{x}), \qquad \mathbf{x} = (x,y,z) \in \Gamma. \tag{8.2}$$

We solve the problem on a sequence of seven polygonal meshes, with decreasing meshsize h, made up with triangles and hexagons whose vertices lie on Γ. These polygonal meshes are constructed with an ad-hoc algorithm starting from a triangulation of the sphere obtained with the MATLAB library DistMesh [49]. Each polygonal mesh has been obtained by the algorithm explained in the previous Section 7.1. The sequence of polygonal meshes is such that in each mesh the ratio between the number of triangles and hexagons is approximately constant and for $h \to 0$, this ratio tends to 12 : 1. Furthermore, the sequence of polygonal meshes fulfils the regularity assumptions (A1)–(A2).

We test the convergence rate as follows. Let u_I be the interpolant, defined in (5.17), of the exact solution u and let $\delta_h := u_I - u_h$. We consider the following approximations of the L^2, L^∞ and H^1 errors, respectively:

$$\mathrm{E}_{\mathrm{L}^2,h} := \langle \delta_h, \delta_h \rangle_{\mathrm{L}^2_h}; \tag{8.3}$$

$$\mathrm{E}_{\mathrm{L}^\infty,h} := \max_{P \in \mathrm{nodes}(\Gamma_h)} |\delta_h|; \tag{8.4}$$

$$\mathrm{E}_{\mathrm{H}^1,h} := a_h(\delta_h, \delta_h), \tag{8.5}$$

where the forms $a_h(\cdot,\cdot)$ and $\langle \cdot,\cdot \rangle_{\mathrm{L}^2_h}$ are defined in (4.15) and (4.19), respectively. These approximations are $\mathcal{O}(h^2)$-accurate, see for instance [4]. The need of defining these approximate norms and seminorms arise from the presence of the virtual basis functions that are not known in closed form. These norms are reminiscent of the approximate L^2 norm used for instance in [4], (Eq. 46), but also account for the fact that, in our case, the exact and the numerical solutions are defined on different surfaces. The convergence rate in the norms and seminorms defined in (8.3)–(8.5) is estimated by computing these errors as functions of h.

The coarsest of the polygonal meshes under consideration (meshsize $h = 0.6209$) is shown in Figure 6a. The numerical solution obtained on the finest mesh (meshsize $h = 0.0798$) is shown in Figure 6b. The convergence results are shown in Figure 6c. The convergence is linear in H^1 norm and, even if the method is not designed for optimal L^2 and L^∞ convergence, it appears to be quadratic in L^2 norm and almost quadratic in L^∞ norm. We remark that the considered meshes, like the one in Figure 6a, have polygons of very different size and shape, this means that the regularity assumptions (A1) and (A2) are quite weak and the method is thus robust with respect to badly shaped meshes.

8.2.2. Experiment 2 (Torus)

In this experiment we solve the Laplace-Beltrami equation

$$\begin{cases} -\Delta_\Gamma u(x,y,z) = \dfrac{100z}{9}\left(2 - \frac{7}{10}(x^2+y^2)^{-\frac{1}{2}}\right), & (x,y,z) \in \Gamma, \\ \int_\Gamma u(x,y,z)\,\mathrm{d}\sigma = 0 \end{cases} \tag{8.6}$$

on the torus $\Gamma := \{(x,y,z) \in \mathbb{R}^3 | ((x^2+y^2)^{\frac{1}{2}} - \frac{7}{10})^2 + z^2 = \frac{9}{100}\}$, whose exact solution is given by $u(x,y,z) = z, \quad (x,y,z) \in \Gamma$. A similar experiment has been considered in [52]. In this case, the Fermi stripe of Γ is $U = \{(x,y,z) \in \mathbb{R}^3 | (x,y) \neq (0,0) \wedge (x^2+y^2 \neq \frac{49}{100} \vee z \neq 0)\}$, that is the whole space deprived of a circle and the z-axis, the oriented distance function is given by $d(\mathbf{x}) = (((x^2+y^2)^{\frac{1}{2}} - \frac{7}{10})^2 + z^2)^{\frac{1}{2}} - \frac{3}{10}$, $\mathbf{x} \in U$ and the outward unit normal vector field is given by $\nu(x,y,z) = \frac{10}{3}(x,y,z) - \frac{35}{3(x^2+y^2)^{\frac{1}{2}}}(x,y,0)$, $(x,y,z) \in \Gamma$. Hence, the representation (2.3) of the tangential gradient of a function $f \in \mathrm{C}^1(\Gamma)$ becomes

$$\nabla_\Gamma f(\mathbf{x}) = \nabla f(\mathbf{x}) - (\nabla f(\mathbf{x}) \cdot \mathbf{x})\mathbf{x} = \begin{bmatrix} 1-\nu_1^2(\mathbf{x}) & -\nu_1(\mathbf{x})\nu_2(\mathbf{x}) & -\nu_1(\mathbf{x})\nu_3(\mathbf{x}) \\ -\nu_1(\mathbf{x})\nu_2(\mathbf{x}) & 1-\nu_2^2(\mathbf{x}) & -\nu_2(\mathbf{x})\nu_3(\mathbf{x}) \\ -\nu_1(\mathbf{x})\nu_3(\mathbf{x}) & -\nu_2(\mathbf{x})\nu_3(\mathbf{x}) & 1-\nu_3^2(\mathbf{x}) \end{bmatrix} \nabla f(\mathbf{x}), \qquad \mathbf{x} \in \Gamma, \tag{8.7}$$

with $\nu(\mathbf{x}) = (\nu_1(\mathbf{x}), \nu_2(\mathbf{x}), \nu_3(\mathbf{x}))$ as defined above.

We consider a family of meshes defined as follows. Given $m, n \in \mathbb{N}$, the approximation Γ_h of the torus Γ is the polytope having the following mn gridpoints as vertices

$$P_{ij} = \left(\left(\frac{7}{10} + \frac{3}{10}\cos\frac{2i\pi}{n}\right)\cos\frac{2j\pi}{m}, \left(\frac{7}{10} + \frac{3}{10}\cos\frac{2i\pi}{n}\right)\sin\frac{2j\pi}{m}, \frac{3}{10}\sin\frac{2i\pi}{n}\right), \qquad i = 1,\dots n, \quad j = 1,\dots,m,$$

such that a trapezoidal mesh is obtained. To test the convergence, we consider a sequence of six trapezoidal meshes $\Gamma_h^{(k)}$ of the type described above, obtained by increasing $n = 3 \times 2^k$ and $m = 8 \times 2^k$, $k = 0,\dots,5$. The mesh $\Gamma_h^{(2)}$ is shown in Figure 7(a), while the numerical solution obtained for $k = 5$ is shown in Figure 7(b). For all $k = 0,\dots,5$, the errors (8.3)–(8.5) are shown in Figure 7(c) as functions of h. The experimental convergence rate is quadratic in the approximate L^2, L^∞ norms and H^1 seminorm. This superconvergence is due to the symmetry of the mesh and of the solution.

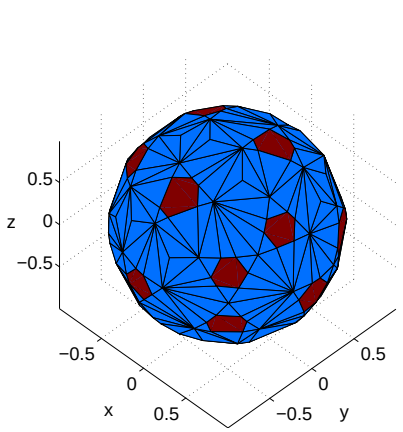

(a) Polygonal approximation Γ_h of the unit sphere Γ, made up of triangles and hexagons, with meshsize $h = 0.6209$.

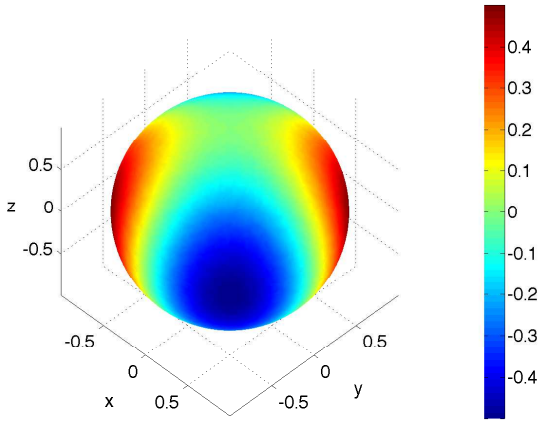

(b) Numerical solution obtained on Γ_h, for $h = 0.0798$.

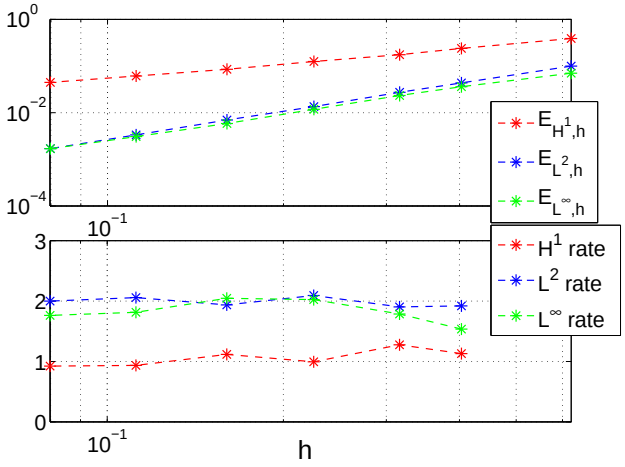

(c) Convergence results

FIGURE 6. Experiment 1 on the unit sphere.

8.2.3. Experiment 3 (mesh pasting along a curve)

In this experiment we solve the Laplace-Beltrami equation and we address the problem of pasting two surfaces along a curve. We consider the cylinder

$$\Gamma := \{(x, y, z) \in \mathbb{R}^3 \mid x^2 + y^2 = 1 \wedge 0 \leq z \leq 2\}, \tag{8.8}$$

and we split it into two parts $\Gamma_1 := \Gamma \cap \{z \leq 1\}$ and $\Gamma_2 := \Gamma \cap \{z \geq 1\}$.

We consider the following Laplace-Beltrami problem with Neumann boundary conditions

$$\begin{cases} -\Delta_\Gamma u = ((10 + \pi^2)x^2 - 6x^4 - 6x^2y^2 - 2)\cos(\pi z), & (x, y, z) \in \Gamma, \\ \dfrac{\partial u}{\partial \boldsymbol{n}} = 0, & (x, y, z) \in \partial\Gamma, \\ \int_\Gamma u \mathrm{d}\sigma = 0, \end{cases} \tag{8.9}$$

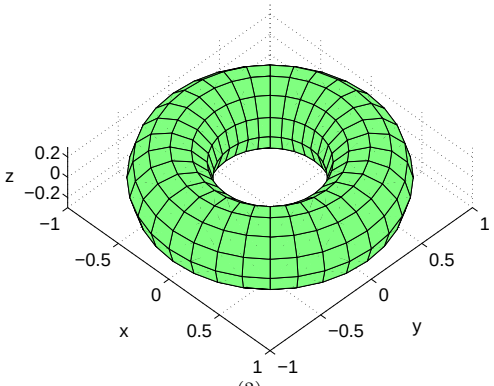

(a) Trapezoidal mesh $\Gamma_h^{(2)}$ for the torus Γ, with meshsize $h = 0.2470$.

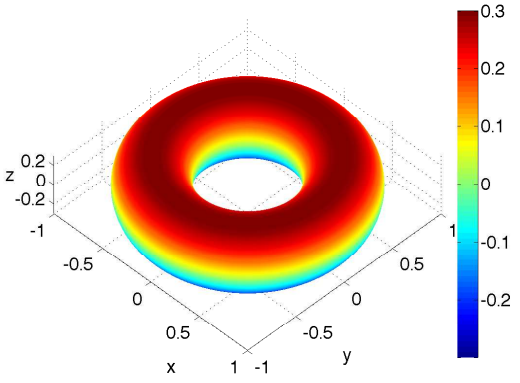

(b) Numerical solution obtained on the finest mesh $\Gamma_h^{(5)}$, with meshsize $h = 0.0314$.

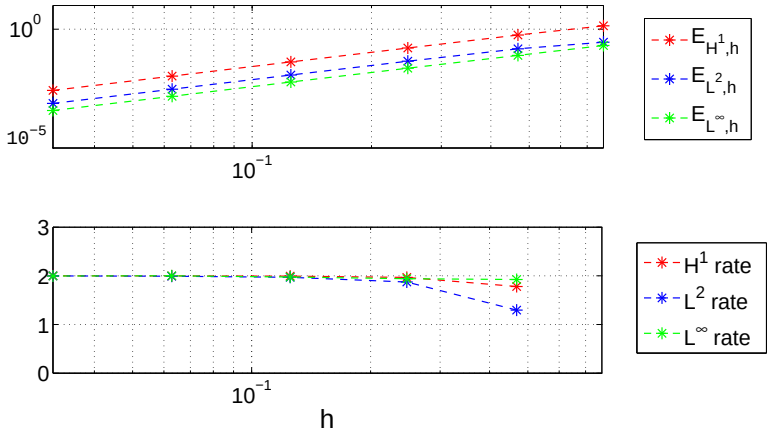

(c) Convergence results

FIGURE 7. Experiment 2 on the torus.

whose exact solution is given by $x(x,y,z) = x^2\cos(\pi z),\ (x,y,z) \in \Gamma$.

In this case, the Fermi stripe of Γ is $U = \{(x,y,z) \in \mathbb{R}^3 | (x,y) \neq (0,0)\}$, the oriented distance function is given by $d(x,y,z) = \sqrt{x^2+y^2} - 1,\ (x,y,z) \in U$ and the outward unit normal vector field is given by $\nu(x,y,z) = (x,y,0),\ (x,y,z) \in \Gamma$. Hence, the representation (2.3) of the tangential gradient of a function $f \in \mathrm{C}^1(\Gamma)$ becomes

$$\nabla_\Gamma f(\mathbf{x}) = \nabla f(\mathbf{x}) - (\nabla f(\mathbf{x}) \cdot (x,y,0))(x,y,0) = \begin{bmatrix} 1-x^2 & -xy & 0 \\ -xy & 1-y^2 & 0 \\ 0 & 0 & 1 \end{bmatrix} \nabla f(\mathbf{x}), \qquad \mathbf{x} = (x,y,z) \in \Gamma. \tag{8.10}$$

We consider a family of meshes defined as follows. Let $n \in \mathbb{N}$. The half cylinder Γ_1 is approximated with $6n^2$ equal rectangular elements having the following $6n(n+1)$ gridpoints as vertices:

$$P_{ij} = \left(\cos\frac{i}{3n}\pi, \sin\frac{i}{3n}\pi, \frac{j}{n}\right), \qquad i = 1, \dots 6n, \quad j = 0, \dots, n,$$

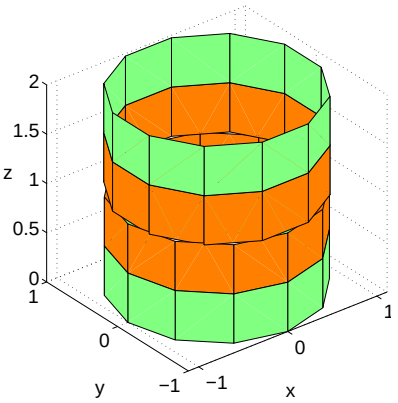

(a) Nonconforming polygonal approximation $\Gamma_h^{(1)}$ of Γ, with meshsize $h = 1.4142$, made up of rectangles and pentagons.

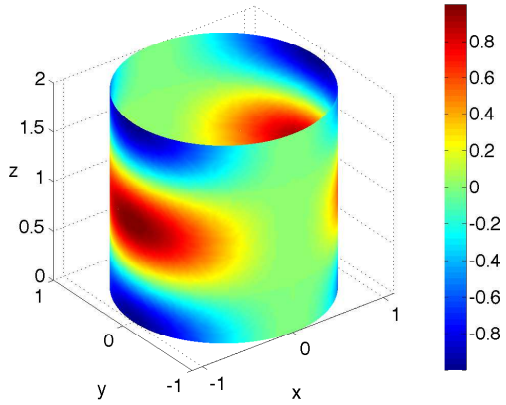

(b) Numerical solution obtained on the finest mesh $\Gamma_h^{(5)}$.

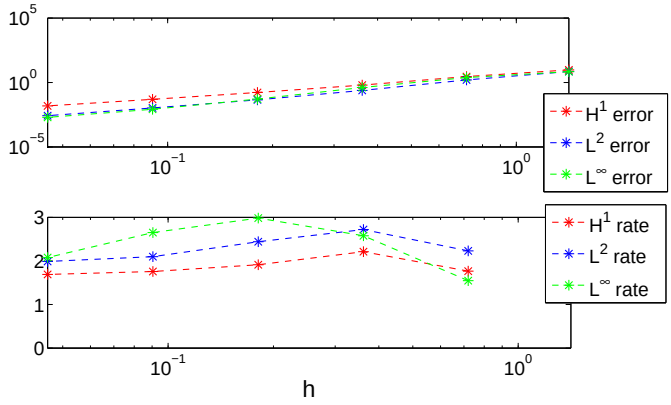

(c) Convergence results.

FIGURE 8. Experiment 3: mesh pasting on the cylinder.

while the half cylinder Γ_2 is approximated with $6n^2$ equal rectangular elements constructed on the following $6n(n+1)$ gridpoints:

$$P_{ij} = \left(\cos\frac{2i+1}{6n}\pi, \sin\frac{2i+1}{6n}\pi, \frac{j}{n}+1\right), \qquad i = 1,\dots 6n \quad j = 0,\dots,n.$$

By pasting these meshes we end up with a nonconforming and discontinuous mesh Γ_h made up of $12n^2$ elements, of which $12n(n-1)$ rectangles and $12n$ degenerate pentagons with one hanging node each.

To test the convergence, we consider a sequence of six meshes $\Gamma_h^{(k)}$ of the type described above, by increasing $n = 2^k$, $k = 0,\dots,5$. Notice that $h = \mathcal{O}(\frac{1}{n})$. For $n = 1$, the nonconforming mesh $\Gamma_h^{(0)}$ is shown in Figure 8(a), in which the rectangles are green and the pentagons are orange, while the corresponding numerical solution on the finest mesh is shown in Figure 8(b).

For all $k = 0,\dots,5$, the errors in the norms and seminorms (8.3)–(8.5) are shown in Figure 8(c) as functions of h. The experimental convergence rate is quadratic in the approximate L^2 and L^∞ norms and superlinear in the approximate H^1 seminorm.

9. Conclusions

In this study, we have considered a Surface Virtual Element Method (SVEM) for the numerical approximation of the Laplace-Beltrami equation on smooth surfaces, by generalising the VEM on planar domains [1] and the Surface FEM [37]. By extending the results in [1, 37], under minimal regularity assumptions for the polygonal approximation of the surface, we have shown optimal asymptotic error estimates, that is: (i) for the interpolation in the SVEM function space, (ii) for the approximation of the surface and (iii) for the projection onto the polygonal surface. In particular, the geometric error arising from the approximation of the surface is quadratic in the meshsize h and then one of the main features of the VEM in the planar case, that is arbitrary order of accuracy on polytopal meshes, cannot be fully exploited when working on surfaces. For this reason, we have confined this study to the case of virtual elements of first polynomial order $k = 1$. In order to increase the convergence rate of the overall method, it is necessary to improve the approximation of geometry. To this end, following [45], curved polygonal elements could be used. This will be subject of future investigations.

In the case $k = 1$, we have also shown existence, uniqueness of the numerical solution and its first order H^1 convergence. Moreover, we have shown (in Sect. 7) the differences, in terms of implementation, between the planar VEM and the SVEM. In particular, we have discussed (i) the construction of test problems on arbitrary surfaces, (ii) the computation of the matrices involved in the method and (iii) how to construct the discrete problem for the Laplace-Beltrami equation as a sparse, full-rank linear system which accounts for the zero-average condition on the solution. We have pointed out the ability of the SVEM to handle nonconforming discontinuous meshes, which is particularly advantageous when applied to mesh pasting, for which the classical SFEM cannot be applied. We have shown the predicted convergence rate of the SFEM in three numerical examples for the Laplace-Beltrami equation (i) on the unit sphere with triangular and hexagonal elements, (ii) on the torus with trapezoidal meshes and (iii) on a cylindrical surface.

Acknowledgements. The authors acknowledge prof. L. Beirão da Veiga for several fruitful discussions during the preparation of the manuscript. Moreover, the authors would like to thank the anonymous referees for their constructive comments and suggestions.

References

[1] L. Beirão da Veiga, F. Brezzi, A. Cangiani, G. Manzini, L.D. Marini and A. Russo, Basic principles of virtual element methods. *Math. Mod. Methods Appl. Sci.* **23** (2013) 199–214.

[2] L. Beirão Da Veiga, F. Brezzi and L.D. Marini, Virtual elements for linear elasticity problems. *SIAM J. Numer. Anal.* **51** (2013) 794–812.

[3] D. Mora, G. Rivera and R. Rodríguez, A virtual element method for the Steklov eigenvalue problem. *Math. Mod. Methods Appl. Sci.* **25** (2015) 1421–1445.

[4] G. Vacca and L. Beirão da Veiga, Virtual element methods for parabolic problems on polygonal meshes. *Numer. Methods Partial Diff. Eq.* **31** (2015) 2110–2134.

[5] G. Vacca, Virtual element methods for hyperbolic problems on polygonal meshes. *Comput. Math. Appl.* **74** (2017) 882–898.

[6] P.F. Antonietti, L. Beirão Da Veiga, S. Scacchi and M. Verani, A C^1 virtual element method for the Cahn-Hilliard equation with polygonal meshes. *SIAM J. Numer. Anal.* **54** (2016) 34–56.

[7] M.F. Benedetto, S. Berrone and S. Scialò, A globally conforming method for solving flow in discrete fracture networks using the virtual element method. *Finite Elements Anal. Design* **109** (2016) 23–36.

[8] L. Beirão da Veiga, F. Brezzi, L.D. Marini and A. Russo, The hitchhiker's guide to the virtual element method. *Math. Mod. Methods Appl. Sci.* **24** (2014) 1541–1573.

[9] B. Ayuso de Dios, K. Lipnikov and G. Manzini, The nonconforming virtual element method. *ESAIM: M2AN* **50** (2016) 879–904.

[10] N. Benkemoun, A. Ibrahimbegovic and J.-B. Colliat, Anisotropic constitutive model of plasticity capable of accounting for details of meso-structure of two-phase composite material. *Comput. Struct.* **90** (2012) 153–162.

[11] J. Chen, A memory efficient discontinuous Galerkin finite-element time-domain scheme for simulations of finite periodic structures. *Microwave Optical Technol. Lett.* **56** (2014) 1929–1933.

[12] T. Kanai, H. Suzuki, J. Mitani and F. Kimura, Interactive mesh fusion based on local 3d metamorphosis. *Graphics Interface* **99** (1999) 148–156.

[13] A. Sharf, M. Blumenkrants, A. Shamir and D. Cohen-Or, Snappaste: an interactive technique for easy mesh composition. *Visual Comput.* **22** (2006) 835–844.

[14] A. Cangiani, E.H. Georgoulis and S. Metcalfe, Adaptive discontinuous Galerkin methods for nonstationary convection–diffusion problems. *IMA J. Numer. Anal.* **34** (2014) 1578–1597.

[15] K.Y. Dai, G.R. Liu and T.T. Nguyen, An n-sided polygonal smoothed finite element method (nSFEM) for solid mechanics. *Finite Elements Anal. Design* **43** (2007) 847–860.

[16] L. Beirão da Veiga and G. Manzini, A virtual element method with arbitrary regularity. *IMA J. Numer. Anal.* **34** (2014) 759–781.

[17] F. Brezzi and L.D. Marini, Virtual element methods for plate bending problems. *Comput. Methods Appl. Mech. Eng.* **253** (2013) 455–462.

[18] N. Flyer and G.B. Wright, Transport schemes on a sphere using radial basis functions. *J. Comput. Phys.* **226** (2007) 1059–1084.

[19] N. Flyer and Grady B. Wright, A radial basis function method for the shallow water equations on a sphere, In *Proc. of the Royal Society of London A: Math., Physical and Engineering Sciences Proc. R. Soc. A* **465** (2009) 1949–1976.

[20] P. Tang, Q. Feng, H. Zhang and Y. Yang, Phase separation patterns for diblock copolymers on spherical surfaces: A finite volume method. *Phys. Rev. E* **72** (2005) 016710.

[21] M. Bertalmıo, L.T. Cheng, S. Osher and G. Sapiro, Variational problems and partial differential equations on implicit surfaces. *J. Comput. Phys.* **174** (2001) 759–780.

[22] M. Bergdorf, I.F. Sbalzarini and P. Koumoutsakos, A lagrangian particle method for reaction–diffusion systems on deforming surfaces. *J. Math. Biology* **61** (2010) 649–663.

[23] R. Barreira, Charles M. Elliott and A. Madzvamuse, The surface finite element method for pattern formation on evolving biological surfaces. *J. Math. Biology* **63** (2011) 1095–1119.

[24] E.J. Fuselier and G.B. Wright, A high-order kernel method for diffusion and reaction-diffusion equations on surfaces. *J. Scientific Comput.* **56** (2013) 535–565.

[25] M. Frittelli, A. Madzvamuse, Ivonne Sgura and C. Venkataraman, Preserving invariance properties of reaction-diffusion systems on stationary surfaces. To appear in: *IMA J. Num. Anal.* (2017), drx058.

[26] M.A.J. Chaplain, M. Ganesh and I.G. Graham, Spatio-temporal pattern formation on spherical surfaces: numerical simulation and application to solid tumour growth. *J. Math. Biology* **42** (2001) 387–423.

[27] C.M. Elliott and B. Stinner, Modeling and computation of two phase geometric biomembranes using surface finite elements. *J. Comput. Phys.* **229** (2010) 6585–6612.

[28] C.M. Elliott, B. Stinner and C. Venkataraman, Modelling cell motility and chemotaxis with evolving surface finite elements. *J. Royal Soc. Interface*, **9** (2012) 3027–3044.

[29] Q. Du and L. Ju, Approximations of a Ginzburg-Landau model for superconducting hollow spheres based on spherical centroidal Voronoi tessellations. *Math. Comput.* **74** 1257–1280 (2005).

[30] C. Eilks and C.M. Elliott, Numerical simulation of dealloying by surface dissolution via the evolving surface finite element method. *J. Comput. Phys.* **227** (2008) 9727–9741.

[31] G. Xu, Q. Pan and C.L. Bajaj, Discrete surface modelling using partial differential equations. *Computer Aided Geometric Design* **23** (2006) 125–145.

[32] M.E. Taylor. Partial differential equations III: Nonlinear Equations, 2nd Ed. Vol 117 of *Applied Math. Sciences*, Springer (2011).

[33] C.B. Macdonald and S.J. Ruuth, The implicit closest point method for the numerical solution of partial differential equations on surfaces. *SIAM J. Sci. Comput.* **31** (2009) 4330–4350.

[34] L. Ju and Q. Du, A finite volume method on general surfaces and its error estimates. *J. Math. Analy. Appl.* **352** (2009) 645–668.

[35] A. Dedner, P. Madhavan and B. Stinner, Anal. of the discontinuous Galerkin method for elliptic problems on surfaces. *IMA J. Numer. Anal.*, (2013) drs033..

[36] J. Giesselmann and T. Müller, Geometric error of finite volume schemes for conservation laws on evolving surfaces. *Numer. Math.* **128** (2014) 489–516.

[37] G. Dziuk and C.M. Elliott, Finite element methods for surface PDEs. *Acta Numer.* **22** (2013) 289–396.

[38] N. Tuncer, A. Madzvamuse and A.J. Meir, Projected finite elements for reaction–diffusion systems on stationary closed surfaces. *Appl. Numer. Math.* **96** (2015) 45–71.

[39] G. Dziuk, Finite elements for the Beltrami operator on arbitrary surfaces. *Partial Diff. Equ. Calcul. Variat.* (1988) 142–155. .

[40] M.E. Taylor. Partial differential equations I: Basic Theory, 2nd Ed., n Vol. 115 of *Series: Appl. Math. Sci.* Springer (2011).

[41] A. Quarteroni and A. Valli. Numerical approximation of partial differential equations. In Vol. 23 of *Springer Science & Business Media* (2008).

[42] B. Ahmad, A. Alsaedi, F. Brezzi, L.D. Marini and A. Russo, Equivalent projectors for virtual element methods. *Comput. Math. Appl.* **66** (2013) 376–391.

[43] S. Brenner and R. Scott. The mathematical theory of finite element methods. In Vol. 15 of , *Springer Science & Business Media* (2007).

[44] P.G. Ciarlet. The finite element method for elliptic problems. SIAM (2002).

[45] A. Demlow, Higher-order finite element methods and pointwise error estimates for elliptic problems on surfaces. *SIAM J. Numer. Anal.* **47** (2009) 805–827.

[46] B. Meyer, On the symmetries of spherical harmonics. *Can. J. Math* **6** (1954) 135–157.

[47] P.-O. Persson. *Mesh generation for implicit geometries*. Ph.D. Thesis, Massachusetts Institute of Technology (2004).

[48] F. Dassi. *Advanced techniques for the generation and the gdaptation of complex surface meshes*. Ph.D. Thesis, Politecnico di Milano (2014).
[49] P.-O. Persson and G. Strang, A simple mesh generator in MATLAB. *SIAM Rev.* **46** (2004) 329–345.
[50] ALBERTA - An adaptive hierarchical finite element toolbox, http://www.alberta-fem.de.
[51] Z. Chen and J. Zou, Finite element methods and their convergence for elliptic and parabolic interface problems. *Numer. Math.* **79** (1998) 175–202.
[52] A. Demlow and G. Dziuk, An adaptive finite element method for the Laplace–Beltrami operator on implicitly defined surfaces. *SIAM J. Numer. Anal.* **45** (2007) 421–442.